Title

Halofuginone, a promising drug for treatment of pulmonary hypertension

Journal

British Journal of Pharmacology, 178(17)

ISSN

0007-1188

Authors

Jain, Pritesh P
Zhao, Tengteng
Xiong, Mingmei
et al.

Publication Date

2021-09-01

DOI

10.1111/bph.15442

Peer reviewed

HHS Public Access

Author manuscript

Br J Pharmacol. Author manuscript; available in PMC 2022 December 26.

Published in final edited form as:

Br J Pharmacol. 2021 September ; 178(17): 3373–3394. doi:10.1111/bph.15442.

Halofuginone, a promising drug for treatment of pulmonary hypertension

Pritesh P. Jain[1], **Tengteng Zhao**[1], **Mingmei Xiong**[1,2], **Shanshan Song**, **Ning Lai**[1,3], **Qiuyu Zheng**[4], **Jiyuan Chen**[1,3], **Shane G. Carr**, **Aleksandra Babicheva**[1], **Amin Izadi**[1], **Marisela Rodriguez**[1], **Shamin Rahimi**[1], **Francesca Balistrieri**[1], **Shayan Rahimi**[1], **Tatum Simonson**[1], **Daniela Valdez-Jasso**[5], **Patricia A. Thistlethwaite**[6], **John Y.-J. Shyy**[7], **Jian Wang**[1,3], **Ayako Makino**[4], **Jason X.-J. Yuan**[1]

[1]Section of Physiology, Division of Pulmonary, Critical Care and Sleep Medicine, Department of Medicine, University of California, San Diego, La Jolla, California, USA

[2]Department of Critical Care Medicine, The Third Affiliated Hospital of Guangzhou Medical University, Guangzhou, China

[3]State Key Laboratory of Respiratory Medicine, The First Affiliated Hospital of Guangzhou Medical University, Guangzhou, China

[4]Division of Endocrinology and Metabolism, University of California, San Diego, La Jolla, California, USA

[5]Department of Bioengineering, University of California, San Diego, La Jolla, California, USA

[6]Division of Cardiothoracic Surgery, Department of Surgery, University of California, San Diego, La Jolla, California, USA

[7]Division of Cardiovascular Medicine, Department of Medicine, University of California, San Diego, La Jolla, California, USA

Abstract

Background and Purpose: Halofuginone is a febrifugine derivative originally isolated from Chinese traditional herb Chang Shan that exhibits anti-hypertrophic, anti-fibrotic and

Correspondence Dr Jason X.-J. Yuan, Section of Physiology, Division of Pulmonary, Critical Care and Sleep Medicine, Department of Medicine, University of California, San Diego, 9500 Gilman Drive, MC 0856, La Jolla, CA 92093-0856, USA. jxyuan@ucsd.edu.

AUTHOR CONTRIBUTIONS

J.X.-J.Y. initiated the project and designed the study. P.P.J. wrote the initial draft of the manuscript. P.P.J., M.X., N.L., Q.Z., J.C. and A.I. performed the animal experiments and analysed the data. T.Z., S.S., A.B. and S.G.C. performed the molecular functional experiments and analysed the data. M.R., Shamin Rahimi, F.B. and Shayan Rahimi contributed in editing the manuscript. T.S., D.V.-J., P.A.T., J.Y.-J.S., A.M. and J.W. participated in the discussion on experimental design and critically reviewed the manuscript.

CONFLICT OF INTEREST

The authors declare no conflicts of interest.

DECLARATION OF TRANSPARENCY AND SCIENTIFIC RIGOUR

This Declaration acknowledges that this paper adheres to the principles for transparent reporting and scientific rigour of preclinical research as stated in the *BJP* guidelines for Design & Analysis, Immunoblotting and Immunochemistry, and Animal Experimentation and as recommended by funding agencies, publishers and other organizations engaged with supporting research.

anti-proliferative effects. We sought to investigate whether halofuginone induced pulmonary vasodilation and attenuates chronic hypoxia-induced pulmonary hypertension (HPH).

Experimental Approach: Patch-clamp experiments were conducted to examine the activity of voltage-dependent Ca^{2+} channels (VDCCs) in pulmonary artery smooth muscle cells (PASMCs). Digital fluorescence microscopy was used to measure intracellular Ca^{2+} concentration in PASMCs. Isolated perfused and ventilated mouse lungs were used to measure pulmonary artery pressure (PAP). Mice exposed to hypoxia (10% O_2) for 4 weeks were used as model of HPH for in vivo experiments.

Key Results: Halofuginone increased voltage-gated K^+ (K_v) currents in PASMCs and K^+ currents through KCNA5 channels in HEK cells transfected with *KCNA5* gene. HF (0.03–1 μM) inhibited receptor-operated Ca^{2+} entry in HEK cells transfected with calcium-sensing receptor gene and attenuated store-operated Ca^{2+} entry in PASMCs. Acute (3–5 min) intrapulmonary application of halofuginone significantly and reversibly inhibited alveolar hypoxia-induced pulmonary vasoconstriction dose-dependently (0.1–10 μM). Intraperitoneal administration of halofuginone (0.3 $mg \cdot kg^{-1}$, for 2 weeks) partly reversed established PH in mice.

Conclusion and Implications: Halofuginone is a potent pulmonary vasodilator by activating K_v channels and blocking VDCC and receptor-operated and store-operated Ca^{2+} channels in PASMCs. The therapeutic effect of halofuginone on experimental PH is probably due to combination of its vasodilator effects, via inhibition of excitation–contraction coupling and anti-proliferative effects, via inhibition of the PI3K/Akt/mTOR signalling pathway.

Keywords

Pulmonary arterial hypertension; halofuginone; treatment; Ca^{2+} channel; K^+ channel; KCNA5; smooth muscle cell

1 | INTRODUCTION

Halofuginone is a synthetic halogenated derivative of febrifugine, a natural quinazolinone alkaloid originally isolated from the plant *Dichroa febrifuga* (also referred to as the Chinese herb Chang Shan (Pines & Spector, 2015). Halofuginone exerts beneficial effects on the treatment of malaria (Jiang et al., 2005; Samant & Sukhthankar, 2009), cancer (Elkin et al., 1999), heart failure (Qin et al., 2017) and fibrosis-related autoimmune diseases (Nagler et al., 1996; Pines, 2014). In a scleroderma clinical trial, a topical formulation of halofuginone improved the mean total skin score, which was used to evaluate the severity of disease (Pines et al., 2003). At the cellular and molecular level, halofuginone has been shown to have an anti-proliferative effect on cancer cells (Grudzien et al., 2010).

Sustained pulmonary vasoconstriction due to pulmonary artery smooth muscle cell (PASMC) contraction and concentric pulmonary vascular remodelling due to PASMC proliferation and migration contribute to the elevated pulmonary vascular resistance and pulmonary artery pressure (PAP) in patients with pulmonary arterial hypertension (PAH) and animals with experimental pulmonary hypertension (PH). Current medical therapies for PAH include IP receptor agonists, such as prostacyclin and its analogues, ET_A/ET_B receptor antagonists such as bosentan and ambrisentan, voltage-dependent Ca^{2+} channel (VDCC)

blockers such as nifedipine and verapamil, soluble guanylate cyclase (sGC) stimulators such as riociguat and PDE inhibitors such as sildenafil (Galie et al., 2015). Recently, clinical trials, along with in vivo animal experiments and in vitro experiments using tissue and cells isolated from PAH patients, have also disclosed that tyrosine kinase receptor antagonists such as imatinib (Hoeper et al., 2013; Quatredeniers et al., 2019), 5-HT receptor and transporter inhibitors (MacLean, 2018) and intravascular pulmonary artery (PA) denervation (Rothman et al., 2020) have beneficial or therapeutic effects on PAH or experimental PH. In addition, many repurposed drugs (Prins et al., 2019), such as digoxin (by inhibiting hypoxia-inducible factor-α) (Abud et al., 2012), rapamycin (by inhibiting mTORC1) (Houssaini et al., 2013), dehydroepiandrosterone (DHEA, by activating Ca^{2+}-activated K^+ channels and inhibiting oxidative stress) (Alzoubi et al., 2013; Krick et al., 2002; Paulin et al., 2011; Prins et al., 2019) and metformin (by activating AMP kinase) (Shang et al., 2016; Zhang et al., 2018), are all proven to have a beneficial effect on experimental PH (Prins et al., 2019). A more effective drug for the treatment of PAH, for example, prostacyclin (PGI_2), is one that affects multiple targets or signalling pathways to achieve its therapeutic effects (Lindegaard Pedersen et al., 2019). Searching for or developing new and effective drugs that can reverse established experimental PH by affecting multiple targets and different signalling pathways is an unfinished task in the research field of the pulmonary circulation and lung vascular disease. Halofuginone is potentially a new drug for the treatment of idiopathic and associated PAH and PH due to lung diseases and/or hypoxia.

An increase in cytosolic free Ca^{2+} concentration ($[Ca^{2+}]_{cyt}$) in PASMCs is a major trigger for pulmonary vasoconstriction and an important stimulus for PASMC proliferation and migration, and subsequent pulmonary vascular remodelling. Sustained pulmonary vasoconstriction and concentric pulmonary vascular remodelling (or concentric wall thickening) both contribute to the development and progression of PAH (Kuhr et al., 2012; Sakao et al., 2015; Tuder et al., 2013). Up-regulated cation channels and enhanced Ca^{2+} influx through different Ca^{2+}-permeable cation channels including VDCCs, receptor-operated Ca^{2+} channels (ROCCs) and store-operated Ca^{2+} channels (SOCCs) in PASMCs have been implicated in the development of idiopathic PAH (Golovina et al., 2001; Lin et al., 2004; Song et al., 2011; Yu et al., 2009). Furthermore, down-regulation or dysfunction of K^+ channels and membrane depolarization are reported to enhance voltage-dependent Ca^{2+} entry and cause pulmonary vasoconstriction and vascular remodelling in patients with PAH and animals with experimental PH (Bonnet et al., 2006; Weir et al., 2008; Yuan et al., 1998).

In this study, we sought to investigate whether acute treatment with halofuginone affects the function of Ca^{2+} and K^+ channels in PASMCs and induces pulmonary vasodilation in isolated lungs and if chronic treatment with halofuginone would ameliorate established experimental PH via regression of the remodelled pulmonary vasculature in mice.

2 | METHODS

2.1 | In vivo animal experiments

All animal care and experimental procedures were approved by the Institutional Animal Care and Use Committee (IACUC) of the University of California, San Diego (Protocol No. S18205) and were performed according to the university and the Institutional Animal

Care and Use Committee (IACUC) guidelines that comply with national and international regulations. Animal studies are reported in compliance with the ARRIVE guidelines (Percie du Sert et al., 2020) and with the recommendations made by the *British Journal of Pharmacology* (Lilley et al., 2020). C57Bl/6 mice (male, 8 weeks old and ~25 g of body weight) purchased from The Jackson Laboratory were placed in standard cages under 12-h light and dark cycles provided with standard chow feed and tap water ad libitum. These mice were used for measuring pulmonary haemodynamics in intact animals, vascular reactivity in isolated perfused and ventilated lungs and lung vascular structural changes in lung angiograms.

The hypoxia-induced PH mouse model was established by exposing mice to 10% O_2 (PO_2 is approximately 71 mmHg) in a normobaric hypoxic chamber (BioSpherix, Lacona, NY) for 4 weeks. The O_2 level in the chamber was continuously monitored by a Proox Model P110 oxygen sensor (BioSpherix) and maintained at 10% by flushing 100% N_2 into the chamber. The normoxic control mice were housed in the same room (21% O_2) but outside the hypoxic chamber. The bedding of the animal cages, as well as water and food for the animals, were replaced once a week.

Animal experiments were designed to have groups of equal size using randomized and blinded analysis. In some instance, however, group sizes were unequal due to unexpected loss of animals while conducting the procedures. In this study, we used the reversal experimental protocol to examine the effect of halofuginone on established experimental PH (or hypoxia-induced PH [HPH]). Mice were first randomly divided into four experimental groups: (i) normoxia + vehicle group ($n = 10$), (ii) hypoxia + vehicle group ($n = 9$), (iii) hypoxia group with intraperitoneal injection of 0.15 $mg \cdot kg^{-1}$, once a day (q.d.), of halofuginone (Hyp + HF-0.15) ($n = 8$) and (iv) hypoxia group with intraperitoneal injection of 0.3 $mg \cdot kg^{-1}$ (q.d.) of halofuginone (Hyp + HF-0.3) ($n = 7$). Halofuginone was injected per day (0.15 and 0.3 $mg \cdot kg^{-1} \cdot day^{-1}$), for 2 weeks after 4 weeks of hypoxic exposure. To examine whether halofuginone affects pulmonary haemodynamics in normoxia control group, we injected 0.3-$mg \cdot kg^{-1}$ halofuginone (i.p., q.d., for 2 weeks) and measured RVP and RV- ± dP/dt. The total duration of hypoxic exposure was 6 weeks, first 4 weeks to establish HPH and then 2 weeks for halofuginone treatment. In hypoxia + vehicle group, the equivalent amount of vehicle (DMSO) was injected i.p. to mice once a day for 2 weeks after 4 weeks of hypoxic exposure. Following haemodynamic measurements, two sets of experiments were performed to measure Fulton index using the heart and conduct angiography experiments using the lungs.

All mice were weighed before experiments. After hypoxic exposure and treatment with halofuginone mice were anaesthetized by inhaling 1.5% isoflurane. Right heart catheterization was performed by introducing a highly sensitive Millar pressure catheter (PVR1030, 1F, Millar Instruments, Colorado, USA) through the external right jugular vein. A baseline calibration was performed for each mouse to ensure that the pressure measured by the catheter was 0 at the beginning of measurements. Right ventricular (RV) pressure (RVP) and RV contractility (RV- ± dP/dt) were measured continuously by the Millar pressure catheter, recorded and analysed by the LabChart software (ADInstruments, Colorado, USA). The mean systemic arterial pressure (mSAP) was continuously measured

by a Millar pressure catheter (ADInstruments, Colorado, USA) positioned in the left carotid artery and monitored using the Millar data acquisition system (ADInstruments, Colorado, USA). The mean PAP (mPAP) was estimated by the value of RV systolic pressure (RVSP) using the formula: mPAP = 0.61 × RVSP + 2 (in mmHg) (Chemla et al., 2004). Following the haemodynamic measurements, pentobarbital (120 $mg \cdot kg^{-1}$) was injected to minimize pain, the heart was carefully isolated, and the right and left atria were carefully removed to measure Fulton index. The right ventricle was precisely excised from the left ventricle (LV) and septum (S) and weighed immediately to avoid drying of tissue. The ratio of the weight of RV to the weight of LV and S [RV/(LV + S)], also referred to as Fulton index, was measured for each mouse to indicate RV hypertrophy.

2.2 | Measurement of PAP in isolated, perfused and ventilated mouse lung

PAP was measured in isolated perfused and ventilated mouse lungs as described previously (Jain et al., 2020; Yoo et al., 2013). Briefly, C57BL/6 mice were anaesthetized with pentobarbital sodium (120 $mg \cdot kg^{-1}$, i.p.), and the trachea was immediately intubated and lungs ventilated with a normoxic gas mixture (21% O_2, 5% CO_2 and balanced N_2) using a miniventilator (Minivent 845, Harvard Apparatus, Holliston, MA, USA). Heparin was injected into the right ventricle to prevent clotting in the pulmonary circulation. A stainless steel catheter was inserted to the main PA via RV. PAP was continuously measured by a pressure sensor (P75 type 379; Hugo Sachs Elektronik-Harvard Apparatus) attached to the PA catheter. A second catheter was introduced in the left heart to drain the perfusate. The lungs were perfused, via the PA catheter, with warm physiological salt solution (PSS, ~37°C) containing 120-mM NaCl, 4.3-mM KCl, 1.8-mM $CaCl_2$, 1.2-mM $MgCl_2$, 19-mM $NaHCO_3$, 1.1-mM KH_2PO_4, 10-mM glucose and 20% FBS (pH 7.4). In the isotonic high K^+ or 40-mM K^+ (40K)-containing solution, equimolar NaCl was replaced by 35.7-mM KCl to maintain the same osmolarity. The PSS perfused the isolated lungs via a peristaltic pump (ISM 834; Ismatec, Glattbrugg, Switzerland) at a flow rate of 1 $ml \cdot min^{-1}$. To achieve a stable baseline of PAP, the lung was first challenged by perfusing 40K-containing solution through the PA catheter three times (3 min for each time), while the lung was ventilated with normoxic gas mixture. To elicit a hypoxic response, the lungs was ventilated with a hypoxic gas mixture (1% O_2, 5% CO_2 and balanced with N_2) for 4 min to achieve a stable or sustained increase in PAP. PowerLab 8/30 and LabChart (ADInstruments, USA) were used for data acquisition and data storage.

2.3 | Mouse lung angiography

Lung angiograms were used to estimate pulmonary vascular remodelling in mice as described previously (Jain et al., 2020; Smith et al., 2015). After haemodynamic measurements, angiography experiments were performed on a second set of C57B1/6 mice. Mice were first randomly divided into four experimental groups: (i) normoxia + vehicle group (Nor), (ii) normoxia + HF group with intraperitoneal injection of 0.3-$mg \cdot kg^{-1}$ halofuginone (q.d.) (Nor + HF), (iii) hypoxia + vehicle group (Hyp) and (iv) hypoxia + HF group with intraperitoneal injection of 0.3-$mg \cdot kg^{-1}$ halofuginone (q.d.) (Hyp + HF-0.3); n = 5 mice in each group. The mice were anaesthetized by pentobarbital sodium (120 $mg \cdot kg^{-1}$, i.p.). The chest was opened by a median sternotomy, and heparin (20 IU) was immediately injected into RV to prevent blood clotting in the pulmonary vasculature. A polyethylene tube

(PE-20, BD Instramedic™ PE Tubing) was inserted into the main PA through RV, and the PBS (pH = 7.4, at 36–38°C) was perfused into the PA at a flow of 0.05 ml·min^{-1} for 3 min to wash out residual blood and blood clots in the pulmonary vasculature. Then, a casting polymer, MICROFIL® (MV-122, Flow Tech, Inc., Carver, MA), was superfused into the PA using an automatic syringe pump (Farmingdale, New York, USA) at the same speed for 1–2 min until the whole lungs were filled with the casting polymer. The MICROFIL-filled lungs were then carefully isolated and stored overnight at 4°C. The next day, dehydration was performed for the MICROFIL-filled lungs using different concentrations of ethanol (50%, 70%, 80%, 95% and 100%, twice for each concentration per hour) to show the lung vasculature. Following the dehydration, the lungs were placed in methyl salicylate on a shaker overnight. The dehydrated MICROFIL-filled lungs were then photographed with a digital camera (MU1000, FMA050, AmScope, CA, USA) through a dissecting microscope (WILD M651, Leica, Switzerland). The periphery of the left lung (1 mm from the edge) vascular image from the apical, middle and basal regions was selected with Adobe Photoshop software and converted to binary images using NIH ImageJ software to quantify the total length of lung vascular branches, the number of vascular branches and the number of vascular branch junctions at a given area. Angiography analysis was not blinded.

2.4 | Cell culture and transfection

Normal human PASMCs (Lonza, RRID:SCR_000377) were cultured in smooth muscle growth medium (SMGM, Lonza), whereas HEK-293 cells were cultured in high-glucose DMEM (Invitrogen) supplemented with 10% FBS (Invitrogen), 100-IU·ml^{-1} penicillin and 100-μg·ml^{-1} streptomycin (Sigma-Aldrich). Cells were maintained in a humidified environment at 37°C and 5% CO_2. Upon reaching 70–90% confluence, cells were detached with trypsin and plated on 25-mm coverslips for electrophysiological and in 60-mm Petri dish for Western blot experiments. The next day, HEK-293 (RRID:CVCL_0045) cells were transiently transfected with 2 μg of human KCNA5 construct (Plasmid No, RG219793; OriGene, Rockville, MD) using X-tremeGENE 9 DNA Transfection Reagent (Roche, Basel, Switzerland) for 4–6 h in Opti-MEM Reduced Serum Medium (Gibco). Then, the Opti-MEM medium was replaced with 10% FBS DMEM. Forty-eight to 72 h later, cells were collected for protein isolation or were used for electrophysiological experiments. The transfection efficiency was confirmed by Western blot.

2.5 | Western blot analysis

The Immuno-related procedures used comply with the recommendations made by the *British Journal of Pharmacology* (Alexander et al., 2018). HEK-293 cells (transfected with KCNA5) and human PASMCs were washed with warm PBS and resuspended into 1× RIPA buffer (Millipore) supplemented with protease inhibitor cocktail tablet (Roche) followed by the incubation on ice for 20 min. The suspensions were centrifuged at 8050 g for 15 min at 4°C. The supernatants were collected, and protein concentrations were measured by a NanoDrop spectrophotometer (Thermo Scientific, USA). Cell lysates with equal quantities of protein were heated at 100°C for 7 min in 6× SDS sample buffer (Boston BioProducts), loaded into 4–12% Bolt™ Bis-Tris Plus polyacrylamide gel (Invitrogen) for electrophoretic separation and transferred to nitrocellulose membrane (Millipore) in Mini Gel Tank apparatus Invitrogen) under conditions recommended by the manufacturer. The

membranes were blocked in 5% non-fat milk (in 1× TBS containing 0.1% Tween 20) for 1 h at room temperature and incubated overnight at 4°C with primary antibodies for KCNA5 (Santa Cruz Biotechnology, Cat. No. sc-25681, RRID:AB_2133661), phosphorylated mTOR (pmTOR) (Cell Signaling Technology, Cat. No. 2971S, 1:1000, RRID:AB_330970), phosphorylated AKT (pAKT) (Cell Signaling Technology, Cat. No. 4060S, 1:1000, RRID: AB_2315049), pan-AKT (Cell Signaling Technology, Cat. No. 4691S, 1:1000, RRID:AB_915783) and mTOR (Cell Signaling Technology, Cat. No. 2983S, 1:1000, RRID:AB_2105622). All samples were reprobed for β-actin (Santa Cruz Biotechnology, Cat. No. sc-47778; 1:2000, RRID:AB_626632) as a loading control. At the next day, the membranes were washed and incubated with anti-rabbit (Cell Signaling Technology, Cat. No. 7074S, RRID:AB_2099233) or anti-mouse (Cell Signaling Technology, Cat. No. 7076S, RRID:AB_330924) secondary antibodies for 1 h at room temperature. Blots were developed using the SuperSignal West Pico Chemiluminescent Substrate (Pierce Biotechnology). Band intensity of target proteins was normalized to β-actin and expressed in arbitrary units (a.u.). For Western blot analyses on pAKT, AKT, pmTOR and mTOR, the band intensity of target proteins from cells treated with PDGF-BB in the absence or presence of BAPTA and BAPTA-AM was normalized to the level of control cells (incubated in 0.3% FBS media) and expressed in arbitrary units.

2.6 | Electrophysiological measurement

Whole-cell outward or inward currents were recorded with the patch-clamp technique using an Axopatch-1D amplifier and a DigiData 1322 interface (Molecular Devices). Whole-cell voltage-gated (K_v) currents ($I_{K(V)}$) were recorded from primary human PASMCs and HEK-293 transiently transfected with the human *KCNA5* gene (OriGene), whereas whole-cell Ba^{2+} currents (I_{Ba}) through VDCCs were recorded from human PASMCs. Briefly, a glass coverslip plated with cells was mounted onto a Plexiglas perfusion chamber on the stage of a Nikon inverted microscope. For recording whole-cell $I_{K(V)}$, cells on the coverslip were bathed in Ca^{2+}-free PSS containing 141-mM NaCl, 4.7-mM KCl, 3-mM $MgCl_2$, 10-mM HEPES, 1-mM EGTA and 10 glucose (pH 7.4). The pipette (intracellular) solution contained 135-mM KCl, 4-mM $MgCl_2$, 10-mM HEPES, 10-mM EGTA and 5-mM Na_2ATP (pH 7.2). Ca^{2+}-free extracellular and intracellular solution and EGTA were used to minimize the contribution of Ca^{2+}-activated K^+ currents to the whole-cell K^+ currents. ATP is included in the intracellular solution to minimize the contribution of ATP-sensitive K^+ currents to the whole-cell K^+ currents. Under these conditions, the whole-cell K^+ currents are mainly K_v currents. For recording whole-cell K^+ currents through KCNA5 channels (I_{KCNA5}), we used HEK-293 cells transiently transfected with the human *KCNA5* gene. The same ionic composition of bath (extracellular) and pipette (intracellular) solutions used for recording whole-cell $I_{K(V)}$ in native PASMCs was used to record whole-cell I_{KCNA5} in *KCNA5*-transfected HEK-293 cells. Digital subtraction of the currents ($I_{K(V)}$ in PASMCs or I_{KCNA5} in HEK-293) recorded in cells during the application of halofuginone from the currents recorded in control cells was defined as halofuginone-sensitive $I_{K(V)}$ or I_{KCNA5}. For recording whole-cell I_{Ba} through VDCCs, the extracellular (bath) solution contained 115-mM NaCl, 10-mM $BaCl_2$, 4.7-mM KCl, 0.5-mM $MgCl_2$, 10-mM HEPES and 10-mM glucose (pH 7.4), and the pipette solution contained 130-mM CsCl, 10-mM EGTA, 5-mM Mg-ATP and 10-mM HEPES (pH 7.2). We used Ba^{2+} in the bath (extracellular) solution

as the charge carrier to measure inward currents through VDCCs and Cs^+ in the pipette (intracellular) solution to minimize outward currents through K^+ channels.

Patch pipettes (2–3 MΩ) were fabricated on an electrode puller (Sutter Instrument, Novato, CA) using borosilicate glass tubes and fire polished on a microforge (Narishige Scientific Instruments, Tokyo, Japan). Command voltage protocols and data acquisition were performed using pCLAMP-10 software (Axon Instruments). With the use of the 2–3 MΩ of pipettes, the series resistance was at a range of 4–9 MΩ when the whole-cell configuration was formed. Series resistance compensation was performed in most of the experiments for recording whole-cell currents. Currents were filtered at 1–2 kHz and digitized at 2–5 kHz. Leak and capacitive currents were subtracted using the P/4 protocol in pCLAMP software. To obtain a full scale of current-voltage (*I–V*) relationship curve for whole-cell $I_{K(V)}$ in PASMCs or I_{KCNA5} in *KCNA5*-transfected HEK-293, the cells were depolarized to a series of test potentials (for 300 ms) ranging from −80 to +80 mV (in 20-mV increments) from a holding potential of −70 mV. For the *I–V* curves of whole-cell I_{Ba}, the cells were depolarized to a series of test potentials (for 200 ms) ranging from −40 to +30 mV (in 10-mV increments) from a holding potential of −70 mV. All experiments were performed at room temperature (22–24°C).

2.7 | Measurement of $[Ca^{2+}]_{cyt}$

Digital imaging fluorescence microscopy approach was used to determine $[Ca^{2+}]_{cyt}$ in human PASMCs and HEK-293 cells. PASMCs were grown on glass coverslips (25 mm in diameter). Cells were first incubated with 4-μM Fura-2 acetoxymethyl ester (Fura-2/AM, Invitrogen/Molecular Probes, Eugene, OR) for 60 min at room temperature (22–24°C). Cells loaded with Fura-2/AM were then superfused with HEPES-buffered bath solution for 30 min to washout extracellular Fura-2/AM and allow enough time for intracellular esterase to cleave Fura-2/AM to Fura-2. Cells loaded with Fura-2 were then alternatively illuminated at 340- and 380-nm wavelengths using Xenon lamp (Hamamatsu Photonics, Hamamatsu, Japan) connected to a Nikon inverted fluorescent microscope (Eclipse Ti-E; Nikon, Tokyo, Japan). The fluorescence emitted at 520 nm was captured using EM-CCD camera (Evolve; Photometrics, Tucson, AZ, USA), and the fluorescence intensity was analysed using NIS Elements 3.2 software (Nikon). The ratio of fluorescence intensity (F_{340}/F_{380}) was used to measure $[Ca^{2+}]_{cyt}$ within an area of interest (AOI) in a cell and recorded every 2 s. The HEPES-buffered solution contained 137-mM NaCl, 5.9-mM KCl, 1.8-mM $CaCl_2$, 1.2-mM $MgCl_2$, 14-mM glucose and 10 HEPES (pH, 7.4, by NaOH). The Ca^{2+}-free solution was prepared by replacing 1.8-mM $CaCl_2$ with equimolar $MgCl_2$ and adding 1-mM EGTA to chelate residual Ca^{2+}. All experiments for measuring $[Ca^{2+}]_{cyt}$ were performed at room temperature (22–24°C).

2.8 | Data and statistical analysis

The data and statistical analysis comply with the recommendations of the *British Journal of Pharmacology* on experimental design and analysis in pharmacology (Curtis et al., 2015). Data analysis was performed in a blinded manner wherever possible. Statistical tests were performed using SigmaPlot 11.0 Systat Software (SigmaPlot Inc., Chicago, IL, USA) with group size equal to or more than 5 ($n \geq 5$). *'n'* represents the number of animals in in

vivo experiments or independent experimental values in in vitro experiments. No outliers were removed from the data analysis and presentation. Data are expressed as means ± SEM. Statistical analysis was performed using paired or unpaired Student's *t* test (for two groups) or ANOVA and post hoc tests (Student–Newman–Kuels or Holm–Sidak) (for multiple groups). The post hoc tests were only performed when there was a significant difference between two groups and there was no variance in homogeneity. Differences are considered significant at $P < 0.05$.

2.9 | Materials

All drugs and chemicals were obtained from Sigma-Aldrich unless otherwise stated. Halofuginone (HY-N2584) was obtained from MedChemExpress (MCE, Monmouth Junction, NJ 08852, USA). Halofuginone and BAPTA-AM were dissolved in DMSO, whereas BAPTA was dissolved in distilled water, to make concentrated stock solutions of halofuginone, BAPTA and BAPTA-AM. These concentrated stock solutions were aliquoted and stored at −20°C until the day of experiments.

2.10 | Nomenclature of targets and ligands

Key protein targets and ligands in this article are hyperlinked to corresponding entries in the IUPHAR/BPS Guide to PHARMACOLOGY (http://www.guidetopharmacology.org) and are permanently archived in the Concise Guide to PHARMACOLOGY 2019/20 (Alexander, Christopoulos et al., 2019; Alexander, Fabbro et al., 2019; Alexander, Kelly et al., 2019a, b; Alexander, Mathie et al., 2019).

3 | RESULTS

An increase in $[Ca^{2+}]_{cyt}$ in smooth muscle cells is a major trigger for pulmonary vasoconstriction. Membrane depolarization-induced Ca^{2+} influx through VDCCs is an important trigger for excitation–contraction coupling in vascular smooth muscle cells. Activation of K^+ channels and an increase in outward K^+ currents result in membrane hyperpolarization or repolarization, which can subsequently inhibit Ca^{2+} influx through VDCCs. To test whether halofuginone induces pulmonary vasodilation by activating K^+ channel activity and/or inhibiting Ca^{2+} influx, we first examined the effect of halofuginone on whole-cell K^+ currents and Ca^{2+} currents in PASMCs using patch-clamp techniques and on receptor-operated (ROCE) and store-operated Ca^{2+} entries (SOCE) in PASMCs using digital imaging fluorescence microscopy.

3.1 | Halofuginone reversibly increases whole-cell K^+ currents in PASMCs

Hypoxia decreases K^+ currents in rat PASMCs causing membrane depolarization (Yuan et al., 1993). We first used intracellular (or pipette) and extracellular (or bath) solutions that were suitable to measure whole-cell voltage-gated K^+ (K_v) currents in PASMCs. In these experiments, the contribution of K^+ currents through ATP-sensitive K^+ (K_{ATP}) channels and Ca^{2+}-activated K^+ (K_{Ca}) channels to the whole-cell currents was minimized by including 10-mM ATP and 10-mM EGTA in the pipette solution and Ca^{2+}-free bath solution. Extracellular application of 1-μM halofuginone significantly and reversibly increased the whole-cell K_v currents in PASMCs (Figure 1a-c). The halofuginone -sensitive K_v currents

seemed to be induced by relatively negative potentials (between −40 and −60 mV) (Figure 1d), whereas multiple parameter fitting was required to best fit the activation (sigmoid, four parameters), inactivation (exponential decay, triple, six parameters) and deactivation (sigmoid, three parameters) phases of the halofuginone -activated currents (Figure 1e). These data indicate that halofuginone significantly and reversibly increased whole-cell K_v currents in PASMCs and that several K_v channels contribute to the halofuginone-induced or halofuginone-enhanced K_v currents.

In human and animal PASMCs, many K_v channels are expressed and contribute to the whole-cell K_v currents. We and others previously reported that KCNA5 (or $K_v1.5$) is one of the K_v channels playing an important role in regulating membrane potential and acute hypoxic pulmonary vasoconstriction (HPV) (Archer et al., 1993, 2000; Platoshyn et al., 2006; Post et al., 1995; Yuan, 1995). To examine if halofuginone directly affects KCNA5, we transfected the human *KCNA5* gene to HEK-293 cells. As shown in Figure 2, transient transfection of *KCNA5* into HEK cells generated large K^+ currents upon depolarization from a holding potential of −70 mV to test potentials ranging from −40 to +80 mV (Figure 2a). The current amplitude and density in HEK-293 cells transiently transfected with KCNA5 (2009.0 ± 263.6 pA and 164.5 ± 31.8 pA·pS^{-1} at +80 mV) were approximately 4.8 (current amplitude) and 12.7 (current density) times higher than those in native PASMCs (415.7 ± 12.4 pA and 12.9 ± 0.9 pA·pS^{-1} at +80 mV), respectively. Extracellular application of 1-μM halofuginone reversibly induced a 36% increase in the current amplitude and a 45% increase in the current density (Figure 2a-c). The *I–V* curve of the halofuginone -sensitive KCNA5 currents indicated an activation threshold of around −60 mV (Figure 2d), and the time course showed that halofuginone -induced increase in KCNA5 currents occurred within 1 min and maximized around 5 min after extracellular application of halofuginone (Figure 2e). Western blot experiments confirmed the efficient transfection and expression of KCNA5 in HEK 293 cells (Figure 2f) we used in the experiments. These results indicate that halofuginone significantly and reversibly increases K^+ currents through KCNA5 channels.

3.2 | Halofuginone inhibits Ca^{2+} entry through ROCC, SOCC and VDCC

Agonist ligand- and hypoxia-induced pulmonary vasoconstriction is triggered by an increase in $[Ca^{2+}]_{cyt}$ in PASMCs due to Ca^{2+} influx through various Ca^{2+} channels in the plasma membrane and Ca^{2+} release from the intracellular stores (McDaniel et al., 2001). The Ca^{2+} influx through ROCC and SOCC is involved in pulmonary vasoconstriction induced by vasoactive agonists, such as endothelin-1, 5-HT and Ang II) (Liu et al., 2012; Xia et al., 2013; Yamamura et al., 2011) and acute alveolar hypoxia (Wang et al., 2005, 2006). SOCE and ROCE are also enhanced in PASMCs isolated from rats with chronic HPH (Lin et al., 2004; Tang et al., 2016; Xiao, Su, et al., 2017), whereas VDCCs are up-regulated in pulmonary arteries in mice with HPH (Wan et al., 2013).

The calcium-sensing receptor (CaSR) is a GPCR that is activated by divalent cations such as Ca^{2+} and Mg^{2+} (Bouschet et al., 2008; Magno et al., 2011), and it appears to be involved in the development and progression of PH (Tang et al., 2016) To test if halofuginone affects CaSR-mediated increase in $[Ca^{2+}]_{cyt}$, we first transfected HEK-293 cells with the *CaSR* gene. The CASR-transfected cells were first superfused with Ca^{2+}-free solution, and then

extracellular Ca^{2+}-mediated increase in $[Ca^{2+}]_{cyt}$ through activation of CaSR was induced by application of 1.8-mM Ca^{2+}, as a ligand of CaSR, in the bath solution. Our previous study showed that application of extracellular Ca^{2+} to HEK cells overexpressing CaSR caused oscillatory increases in $[Ca^{2+}]_{cyt}$, whereas the Ca^{2+} oscillation was not present in non-transfected and GFP-transfected control cells (Song et al., 2020). As shown in Figure 3, extracellular application of Ca^{2+} to *CASR*-transfected HEK-293 cells caused an oscillatory increase in $[Ca^{2+}]_{cyt}$ (Figure 3a). Halofuginone caused a concentration-dependent inhibition of the amplitude of extracellular Ca^{2+}-induced oscillatory increase in $[Ca^{2+}]_{cyt}$ (Figure 3a,b) and the concentration–response curve implied that the IC_{50} for halofuginone-induced inhibition on CaSR-mediated Ca^{2+} influx was approximately 0.07 μM (Figure 3b). We also compared the basal $[Ca^{2+}]_{cyt}$ in CASR-transfected HEK-293 cells treated with vehicle and all concentrations of halofuginone (0.03–1 μM). As shown in Figure 3c, halofuginone treatment also decreased basal $[Ca^{2+}]_{cyt}$. These data indicate that halofuginone significantly inhibited the CaSR-mediated increase in $[Ca^{2+}]_{cyt}$ due to ROCE. In these experiments, however, we could not rule out the possibility that halofuginone might also inhibit CaSR-mediated Ca^{2+} mobilization from intracellular Ca^{2+} stores.

We therefore tested the effect of halofuginone on SOCE in native PASMCs. We used cyclopiazonic acid (CPA, 10 μM), a sarcoplasmic/endoplasmic reticulum Ca^{2+} pump (SERCA) inhibitor, to induce intracellular Ca^{2+} store depletion or reduction (Seidler et al., 1989; Wu et al., 2017). Extracellular application of CPA (10 μM) induced an increase in $[Ca^{2+}]_{cyt}$ in the absence of extracellular Ca^{2+} (0Ca) due apparently to Ca^{2+} mobilization or leak from the SR to the cytosol (Figure 3d, left panel). When CPA-mediated increase in $[Ca^{2+}]_{cyt}$ in the absence of extracellular Ca^{2+} returned to the baseline level (i.e., when Ca^{2+} in the SR was depleted), restoration of extracellular Ca^{2+} to 1.8 mM (1.8Ca) caused another increase in $[Ca^{2+}]_{cyt}$ (Figure 3d, left panel), which was due obviously to Ca^{2+} entry through SOCCs (Wu et al., 2017). Treatment of the cells with halofuginone (0.1 μM, for 10 min) had no effect on the increase in $[Ca^{2+}]_{cyt}$ (first peak increase) due to CPA-mediated Ca^{2+} mobilization from the SR, but significantly inhibited the increase in $[Ca^{2+}]_{cyt}$ (second peak increase) due to CPA-mediated Ca^{2+} influx through SOCCs (or SOCE) (Figure 3d, right panel, and Figure 3e). We also compared the basal $[Ca^{2+}]_{cyt}$ in human PASMCs treated with vehicle and 0.1-μM halofuginone. As shown in Figure 3f, halofuginone slightly decreased basal $[Ca^{2+}]_{cyt}$ with no statistical significance. These data indicate that halofuginone inhibits both ROCE and SOCE, but its effect on Ca^{2+} release remains elusive.

To examine the effect of halofuginone on voltage-dependent Ca^{2+} entry, we also measured and compared whole-cell voltage-gated Ca^{2+} (or Ba^{2+}) currents in PASMCs before, during and after extracellular application of halofuginone. In these experiments, we used Ba^{2+} as the charge carrier to indicate VDCC activity because of its high permeability through VDCCs. Extracellular application of 1-μM halofuginone slightly, but with statistical significance, reduced the whole-cell Ba^{2+} currents, elicited by depolarizing the cells from a holding potential −70 mV to a series of test potentials ranging from −40 to +80 mV (Figure 4a,b). The *I–V* curves showed that the activation threshold for the channels was around −30 mV and the maximal currents occurred at +10 mV (Figure 4b). halofuginone reduced the amplitude of the currents but seemed to have little effect on the amplitude and kinetics of the currents (Figure 4c). The averaged data indicated that acute treatment of PASMCs with

halofuginone (1 μM for 10 min) resulted in a 48% decrease of the current amplitude at +10 mV (Figure 4d). The halofuginone-mediated inhibitory effect on VDCCs was associated with an inhibition of high K^+-induced pulmonary vasoconstriction (Figure 4e,f). In isolated perfused and ventilated mouse lungs, intrapulmonary superfusion of solutions containing 40K caused a rapid increase in PAP apparently due to membrane depolarization-induced increase in $[Ca^{2+}]_{cyt}$ in PASMCs. Short-term treatment with halofuginone (1 μM) through intrapulmonary perfusion resulted in a reversible 42% inhibition of 40K-induced increase in PAP (Figure 4e,f). The inhibition of 40K-mediated pulmonary vasoconstriction (or increase in PAP) in isolated lungs was consistent with the reduction of whole-cell voltage-gated Ca^{2+} currents in PASMCs. These data indicate that halofuginone blocks L-type VDCCs, inhibits voltage-gated Ca^{2+} entry and causes pulmonary vasodilation.

3.3 | Halofuginone inhibits acute HPV

Persistent pulmonary vasoconstriction induced by sustained alveolar hypoxia is involved in the increased pulmonary vascular resistance and PAP in patients with obstructive lung diseases (Simonneau et al., 2019), obstructive sleep apnoea (Simonneau et al., 2019) and chronic mountain sickness and in residents living in high altitude (Wilkins et al., 2015). Using isolated perfused and ventilated lung preparations, we examined the effect of halofuginone on alveolar hypoxia-induced increase in PAP due to acute HPV. As shown in Figure 5a, the angiography image of the left lung showed the vascular complexity and density of pulmonary vascular tree (Figure 5a). Intrapulmonary arterial perfusion of vasoconstrictive agent (e.g., 40K-containing solution in this case, Figure 5b) or ventilation of hypoxic gas mixture (e.g., 1% O_2 and 5% CO_2 in N_2) through a tracheal intubation tube caused a rapid increase in PAP in the isolated perfused/ventilated lung (Figure 5b); restoration of intrapulmonary arterial perfusion to PSS or ventilation to normoxic gas (room air, 21% O_2) resulted in a rapid recovery of the increased PAP to the baseline level (Figure 5b). Short-term (10 min) treatment of the isolated perfused and ventilated lungs with halofuginone (through intrapulmonary arterial perfusion) significantly inhibited alveolar hypoxia-induced increase in PAP due to HPV (Figure 5c,d). Perfusion of halofuginone, from 0.1 to 1 μM, provided effective block of HPV (Figure 5e). These data indicate that intrapulmonary arterial perfusion of halofuginone at concentrations between 0.1 and 1 μM inhibited alveolar hypoxia-induced pulmonary vasoconstriction as a result of its inhibitory effect on VDCC and ROCC and augmenting effect on K^+ channels, including KCNA5.

3.4 | Halofuginone inhibits PDGF-mediated phosphorylation of Akt and mTOR in PASMCs

Receptor-mediated Ca^{2+} influx in PASMCs is not only required for agonist-mediated pulmonary vasoconstriction (Wu et al., 2017) but also required for or involved in growth factor-mediated PASMC proliferation and pulmonary vascular remodelling (Rieg et al., 2018; Song et al., 2011; Yamamura et al., 2014). The in vitro and ex vivo experiments shown in this study indicate that halofuginone significantly inhibited Ca^{2+} influx in PASMCs, by indirectly activating K^+ channel activity and directly inhibiting voltage-dependent Ca^{2+} entry, ROCE and SOCE (Figures 1-5). The next set of experiments was designed to examine whether halofuginone -induced inhibitory effect on Ca^{2+} influx was associated with inhibition of intracellular signalling cascades required for PASMC proliferation.

Growth factor-mediated PASMC proliferation is associated with activation of the PI3K/Akt/mTOR pathway (Rieg et al., 2018; Song et al., 2011; Tang et al., 2016), one of the major signalling pathways associated with cell proliferation (Tang et al., 2015; Xiao, Peng, et al., 2017). We used BAPTA, a potent Ca^{2+} chelator, to chelate extracellular Ca^{2+} in the culture media, and BAPTA-AM, a cell-permeant Ca^{2+} chelator, to chelate intracellular Ca^{2+}, to examine the effects of removal or chelation of extracellular and/or intracellular free Ca^{2+} on PDGF-mediated p-Akt and p-mTOR in PASMCs (Song et al., 2016). As shown in Figure 6a, chelation of free Ca^{2+} in extracellular perfusate by BAPTA significantly attenuated the increase in $[Ca^{2+}]_{cyt}$ induced by CPA, a SERCA inhibitor that induces SOCE by passively depleting Ca^{2+} from the intracellular stores. In the presence of extracellular BAPTA, CPA still induced a marked increase in $[Ca^{2+}]_{cyt}$ due to Ca^{2+} mobilization or leakage from the sarcoplasmic/endoplasmic reticulum to the cytosol. In PASMCs pretreated with BAPTA-AM, however, CPA failed to induce any increase in $[Ca^{2+}]_{cyt}$ (Figure 6a,b). These data indicate that BAPTA and BAPTA-AM can efficiently inhibit or abolish increases in cytosolic free $[Ca^{2+}]_{cyt}$.

Chelation of extracellular Ca^{2+} by BAPTA or chelation of intracellular Ca^{2+} by BAPTA-AM significantly inhibited PDGF-mediated increases in p-Akt and p-mTOR in human PASMCs (Figure 6c), whereas treatment of the cells with BAPTA and BAPTA-AM further almost abolished the PDGF-mediated increases in p-Akt and p-mTOR (Figure 6c,d). These results provide compelling evidence that PDGF (and other growth factors)-mediated activation of the Akt/mTOR signalling pathway, indicative of increased p-Akt and p-mTOR, is dependent on Ca^{2+} influx and/or release in PASMCs.

Indeed, treatment of PASMCs with halofuginone (1 μM, for 48 h) significantly inhibited PDGF (10 $ng \cdot ml^{-1}$)-mediated increases in p-Akt/Akt and p-mTOR / mTOR ratios (Figure 6e,f) as well as in p-Akt and p-mTOR (Figure 6g). The inhibitory effect of halofuginone on PDGF-mediated phosphorylation of Akt/mTOR was likely to be due to its inhibitory effect on Ca^{2+} influx in PASMCs. It has to be noted that halofuginone may inhibit Akt and mTOR phosphorylation via other mechanisms (Chen et al., 2015) (Follo et al., 2019). Given that the Akt/mTOR signalling pathway is a major pathway for inducing cell proliferation, the halofuginone -induced inhibitory effect on the Akt/mTOR signalling cascade would attenuate PASMC proliferation and, ultimately, ameliorate pulmonary vascular remodelling or concentric pulmonary arterial medial thickening.

3.5 | Halofuginone partly reversed established experimental PH in mice

Sustained pulmonary vasoconstriction, inhibited vasodilation and concentric pulmonary arterial remodelling all contribute to the elevation of pulmonary vascular resistance and PAP in patients with PAH and animals with experimental PH (Kuhr et al., 2012; Stenmark et al., 2009; Tuder, 2017). In addition to its acute vasodilatory effect, halofuginone may exert a chronic regression effect on remodelled pulmonary vasculature and reverse PH. To test this hypothesis, we conducted a reversal experiment using mice with chronic hypoxia-induced PH. As shown in the experimental protocol (Figure 7a), 8-week-old mice were first divided into four groups: (i) normoxic group (Nor), (ii) hypoxia + vehicle group (Hyp), (iii) hypoxia group with an intraperitoneal injection of 0.15 $mg \cdot kg^{-1}$, q.d., of halofuginone

(Hyp + HF-0.15) and (iv) hypoxia group with an intraperitoneal injection of 0.3 mg·kg^{-1} (q.d.) of halofuginone (Hyp + HF-0.3). The Hyp and Hyp + HF mice were first exposed to normobaric hypoxia (10% O_2) for 4 weeks and then were injected i.p., once a day, with vehicle (in Hyp group), 0.15 mg·kg^{-1} of halofuginone (HyP + HF-0.15) or 0.3 mg·kg^{-1} of HF (Hyp + HF-0.3) for two more weeks under hypoxic conditions before the haemodynamic and angiography measurements were conducted.

Four weeks of exposure to hypoxia significantly increased RVSP, a surrogate measure for pulmonary arterial systolic pressure (Figure 7b,c). Due to the increased RVSP during hypoxia, the RV contractility, indicated by RV- ± dP/dt, was also increased. The RV-dP/dt is a surrogate measure and reliable indicator for RV contractility that increases in response to the elevated PAP (Tabima et al., 2010; Vitali et al., 2014). Injection of halofuginone, i.p. once a day, at a dose of 0.15 mg·kg^{-1}, for 2 weeks did not significantly attenuate the increases in RVSP and estimated mean PAP (mPAP) (Chemla et al., 2004; Parasuraman et al., 2016) (Figure 7b), Fulton index (Figure 7c) and the ratio of weight of RV to the weight of LV and S [RV/(LV + S)] during hypoxia (Figure 7b,c). Although there was a trend for 0.15-mg·kg^{-1} halofuginone to reverse the chronic hypoxia-induced PH, none of the parameters bear statistical significance. Then we repeated the experiments by increasing the dose of halofuginone to 0.3 mg·kg^{-1} (q.d., for 2 weeks) and found that halofuginone at the higher dose significantly ameliorated the chronic hypoxia-induced PH (Figure 7c,d). The data indicated that this dose of halofuginone reversed, at least partly, the established PH (by approximately 50–55% on RVSP and mPAP and more than 90% on Fulton index).

The next set of experiments was designed to repeat and confirm the reversal experimental results (shown in Figure 7) and show whether halofuginone affected pulmonary haemodynamics and lung vascular structure under normoxic conditions. Intraperitoneal injection of 0.3-mg·kg^{-1} halofuginone q.d. for 2 weeks after 4 weeks of exposure to normoxia (room air, 21% O_2) had no significant effect on RVSP, mPAP and heart rate but slightly decreased RV- + dP/dt_{max} (Figure 8a,b). Four weeks of initial hypoxic exposure significantly increased RVSP, mPAP and RV- + dP/dt_{max} (Figure 8a,b). Then, 2 weeks of intraperitoneal injection of halofuginone (0.3 mg·kg^{-1}, q. d.) under hypoxic conditions significantly inhibited hypoxia-induced increases in RVSP and mPAP (Figure 8b). Halofuginone had no effect on heart rate under normoxic or hypoxic conditions (Figure 8b).

In addition to haemodynamics, we also tested the effect of halofuginone on pulmonary vascular remodelling by angiography. Chronic exposure of mice to hypoxia for 4 weeks significantly decreased the total number of lung vascular branches, the number of vascular branches and the number of vascular branch junctions (Figure 8c,d). It must be noted that the decreased number of lung vascular branches does not necessarily mean that the branches were lost during the 4-week exposure to hypoxia. The decreased total number of branches shown in angiogram in chronically hypoxic mice was mainly due to sustained pulmonary vasoconstriction, concentric pulmonary vascular wall thickening and in situ thrombosis that preclude or inhibit the contrast to fill into small pulmonary arteries and arterioles. Intraperitoneal injection of halofuginone (0.3 mg·kg^{-1}, q.d., for 2 weeks) after 4-week normoxic exposure in control groups of mice had no significant effect on the total length of

branches, the number of branches and the number of junctions (Figure 8c,d). Administration of halofuginone (i.p., 0.3 mg·kg^{-1}, q.d., for 2 weeks) after 4-week hypoxic exposure in chronically hypoxic mice reversed the angiography parameters (the total length of branches, the number of branches and the number of junctions) almost back to the normoxic control level. (Figure 8d).

Further, we also tested the effect of halofuginone on mSAP in mice with established experimental PH. As shown in Figure 9, halofuginone treatment (i.p., 0.3-mg·kg^{-1}, q.d., for 1 week) in mice pre-exposed to 4 weeks of hypoxia had little effect on SAP (Figure 9a), LV- + dP/dt_{max} and heart rate (Figure 9b). The same experimental protocol, however, still caused a significant inhibition of RV hypertrophy, as indicated by a decrease of Fulton index (Figure 9c).

These data indicate that halofuginone at the dose of 0.3 mg·kg^{-1} (q.d. and i.p.) was an efficient therapy for experimental PH, inhibiting pulmonary vascular remodelling and vasodilating the pulmonary vasculature. The inhibitory effect of halofuginone on pulmonary haemodynamics and vascular structure was specific to mice with hypoxia-induced PH. Treatment with halofuginone given to mice under normoxic conditions had no effect on RVSP and mPAP, and halofuginone given to mice under hypoxic conditions had little effect on systemic arterial pressure and left ventricular contractility.

4 | DISCUSSION

In this study, we report that (i) acute (5–10 min) treatment with halofuginone significantly and reversibly increased whole-cell K_v currents in PASMCs and K^+ currents through KCNA5 channels in *KCNA5*-transfected HEK-293 cells; (ii) acute treatment with HF inhibited ROCE, specifically, CaSR-associated Ca^{2+} influx, and SOCE, specifically, CPA-mediated Ca^{2+} influx, in PASMCs; (iii) acute halofuginone treatment slightly, but significantly, decreased whole-cell cation currents through VDCCs in PASMCs; (iv) acute (5–10 min) intrapulmonary perfusion of halofuginone significantly inhibited acute alveolar hypoxia-induced pulmonary vasoconstriction and high K^+-mediated pulmonary vasoconstriction; and (v) chronic treatment of mice with i.p. halofuginone partly and significantly reversed established experimental PH, as indicated by improved pulmonary haemodynamics, reduced lung vascular remodelling and inhibited RV hypertrophy.

Febrifugine, along with chloroquine and quinine, is an anti-malarial drug extracted from hydrangea and the Chinese herb *D. febrifuga* Lour, which belongs to the Saxifragaceae family of herbaceous perennial flowering plants. Extracts from either the roots or the leaves are effective for treating chicks infected with *Plasmodium gallinaceum* and in clinical cases of malaria (Leiba et al., 2006). The active quinazoline-type alkaloid isolated from the roots, with the molecular structure $C_{16}H_{21}0_3N_3$, is designated as febrifugine (Koepfli et al., 1947). Halofuginone is a halogenated derivative of febrifugine and a Food and Drug Administration (FDA)-approved drug for treatment of scleroderma (Pines et al., 2003). Halofuginone also has therapeutic potential on autoimmune disease (Leiba et al., 2006), ischaemic retinal degenerative disease (Kunimi et al., 2019) and cancer (Elkin et al., 1999) based on its

anti-inflammatory, anti-fibrotic and anti-proliferative effects (Grudzien et al., 2010; Nagler et al., 1996; Sundrud et al., 2009).

The anti-malarial effect of febrifugine and its analogues is due, at least in part, to the interaction with prolyl-tRNA synthetase (ProRS) in the blood stage of infection. Halofuginone inhibits ProRS activity causing intracellular accumulation of uncharged tRNA and this action requires ATP (Zhou et al., 2013). Halofuginone also exerts anti-fibrotic effect by reducing collagen synthesis and increasing collagenase activity (Popov et al., 2006) in mice and rats with various fibrotic diseases (Levi-Schaffer et al., 1996; Pines et al., 2001) including pulmonary fibrosis (Nagler et al., 1996, 1998, 1999, 2000) (Gnainsky et al., 2004; Zion et al., 2009). Halofuginone, as shown in in vitro experiments, reduces Smad3 protein (Nelson et al., 2012), inhibits TGF-β-dependent Smad3 phosphorylation and up-regulates expression of the inhibitory Smad7 in a variety of cell types (Gnainsky et al., 2007; Roffe et al., 2010; Zion et al., 2009). The inhibition of Smad3 phosphorylation is due partly to halofuginone -dependent activation of Akt, ERK and p38 MAPK phosphorylation (Roffe et al., 2010). Halofuginone also inhibited endothelial cell MMP-2 expression, basement membrane invasion, capillary tube formation and vascular sprouting, as well as deposition of subendothelial ECM in vitro. In addition, halofuginone inhibits tumour angiogenesis and metastasis in vivo and in vitro (Juarez et al., 2012; Sheffer et al., 2007; Spector et al., 2012; Taras et al., 2006). Furthermore, halofuginone induces myofibroblast and melanoma cell apoptosis (Juarez et al., 2012; Spector et al., 2012) by inhibiting Smad3 phosphorylation downstream of the TGF-β pathway. However, halofuginone also decreases apoptosis of the satellite cells that can re-enter the cell cycle to proliferate and differentiate into myoblasts, which is associated with a decrease in the Bax/Bcl2 ratio (Bodanovsky et al., 2014). Halofuginone inhibits cobalt-mediated increase in HIF-1α (Kunimi et al., 2019) and inhibits NF-κB/p38 MAPK (Leiba et al., 2006) signalling pathways to inhibit cancer cell proliferation. Halofuginone also activates the amino acid response (AAR) by mimicking proline deprivation, protects against renal ischaemic injury and inhibits inflammation (Sundrud et al., 2009). The effects of halofuginone on Th17 differentiation involve increased signalling of ERK and down-regulated expression of STAT3 and NFATc1 (Park et al., 2014).

The observations from this study indicated that halofuginone significantly and reversibly enhanced whole-cell $K_V1.5$/KCNA5 currents and decreased whole-cell cation currents through VDCCs in PASMCs. Halofuginone-induced increase in $I_{K(V)}$ or I_{KCNAS} can lead to membrane hyperpolarization or repolarization, which subsequently decreases the open probability of VDCC. The halofuginone-induced inhibition of whole-cell Ba^{2+} currents through VDCCs in human PASMCs when membrane potential was clamped using the whole-cell configuration of patch-clamp techniques indicates that halofuginone also exerts an inhibitory effect on VDCCs that is independent of membrane potential change. The opposite effect of halofuginone on K_v channels (increasing the channel activity) and VDCCs (decreasing the channel activity) in human PASMCs suggests that halofuginone is an ideal drug for PAH or experimental PH by inducing pulmonary vasodilation and/or inhibiting sustained pulmonary vasoconstriction. Activity of L-type and T-type VDCCs has been implied not only in excitation–contraction coupling for vascular smooth muscle but also in smooth muscle cell proliferation and migration (Fleischmann et al., 1994; Hirenallur et al., 2008; Kuga et al., 1996; Nelson & Quayle, 1995). In addition to inhibiting Ca^{2+} influx

through VDCCs, halofuginone also exerted an acute inhibitory effect on ROCE induced by activation of CaSR and SOCE induced by passive store depletion (using CPA). These data seem to suggest that halofuginone has a non-selective inhibitory effect on different Ca^{2+}-permeable cation channels in PASMCs including VDCC, ROCC and SOCC. It is unclear whether and how halofuginone affects specific channel subunits in these three categories of cation channels.

The halofuginone-mediated inhibition of Ca^{2+} influx or increase in $[Ca^{2+}]_{cyt}$ in PASMCs results in pulmonary vasodilation and inhibition of pulmonary vasoconstriction. In our in vitro experiments, we also found that halofuginone inhibited PDGF-mediated phosphorylation of Akt and mTOR in human PASMCs. The PI3K/Akt/mTOR signalling pathway is one of the major pathways controlling or regulating cell proliferation and protein expression in a variety of cell types (Sourbier et al., 2006; Woo et al., 2017; Xu et al., 2020). We and others have shown that the PI3K/Akt1/mTORC1 pathway is an important signalling pathway associated with pulmonary vascular remodelling in animals with experimental PH, due to its critical role in regulating PASMC (and other types of lung vascular cell) proliferation (Goncharov et al., 2014; Kudryashova et al., 2015; Tang et al., 2015, 2018). The inhibitory effect of halofuginone on PDGF-mediated and Ca^{2+}-sensitive activation or phosphorylation of Akt and mTOR might be due indirectly to its inhibitory effect on Ca^{2+} influx through various Ca^{2+} channels and/or directly to its inhibitory effect on receptor kinase activity (Juarez et al., 2017). Further studies are required to define the pharmacological mechanisms by which halofuginone decreases Akt/mTOR phosphorylation in human PASMCs.

Based on pharmacokinetic and pharmacodynamic studies, Stecklair et al. (2001) reported that i.p. injection of 1.5 $mg{\cdot}kg^{-1}$ of halofuginone in mice resulted in peak plasma halofuginone concentrations between 173 and 209 $ng{\cdot}ml^{-1}$. Using a non-compartmental pharmacokinetic model, the AUC of halofuginone produced by a dose of 1.5 $mg{\cdot}kg^{-1}$ given i.p., was 21,626 $ng{\cdot}ml^{-1}{\cdot}min^{-1}$, thus indicating a bioavailability of 100%. halofuginone after oral administration was undetectable in plasma indicating limited oral bioavailability (Stecklair et al., 2001). The study by Stecklair et al. (2001) also demonstrated that halofuginone doses greater than 1.5 $mg{\cdot}kg^{-1}$ showed significant toxicity in mice. It has been previously reported that i.p. doses of halofuginone between 50 and 300 $\mu g{\cdot}kg^{-1}$ exhibited significant anti-tumour effects with no significant toxicity (de Figueiredo-Pontes et al., 2011). Some studies have further reported that using halofuginone doses between 5 and 400 $ng{\cdot}ml^{-1}$ inhibits angiogenesis in vitro (Elkin et al., 2000) and T-cell activation (Leiba et al., 2006). Recently, it has been shown that halofuginone has therapeutic potential in a mouse model of chronic periodontitis using doses between 0.1 and 1 mg (Wang et al., 2020). Thus, the doses we used for our in vitro and in vivo experiments were within the range previously reported.

The in vivo pharmacological experiments showed that halofuginone at 0.3-$mg{\cdot}kg^{-1}$ (i.p. and q.d.) could efficiently ameliorate experimental PH in mice by improving pulmonary haemodynamics, regressing pulmonary vascular remodelling and attenuating RV hypertrophy. The partial reversal, by halofuginone, of hypoxia-induced PH in mice was believed to result from its combined vasodilative and anti-proliferative effects on the

pulmonary vasculature. The halofuginone -mediated activation of K^+ channels or increase in whole-cell K^+ currents or K^+ efflux may contribute not only to inducing membrane hyperpolarization/repolarization and inhibiting excitation-contraction coupling in pulmonary arterial smooth muscle but also to promoting apoptotic volume decrease (AVD) and apoptosis in PASMCs, causing regression of pulmonary vascular remodelling (Chu et al., 2013). Halofuginone-mediated inhibition of voltage-dependent Ca^{2+} entry, ROCE and SOCE in PASMCs contribute directly to attenuating Ca^{2+}-mediated PASMC contraction and migration (Jin et al., 2014) as well as Ca^{2+}/calmodulin (CaM)-dependent PASMC proliferation (Chu et al., 2013). There are four steps in the cell cycle that are Ca^{2+}/CaM dependent: transition from G_0 phase to G_1 phase, transition from G_1 to S (DNA synthesis) phase, transition from G_2 to M (mitosis) phase and the entire mitosis phase (Kahl & Means, 2003). In addition, a rise in cytosolic and nuclear Ca^{2+} is also an initial stimulus for many signalling proteins and transcription factors, such as CaMK, MAPK, NFAT, CREB, AP-1 and NF-κB that are associated with cell proliferation (Berridge, 1995; Graef et al., 2001; Sheng et al., 1990). Therefore, halofuginone -mediated inhibition of Ca^{2+} influx through various Ca^{2+}-permeable cation channels would result efficiently in inhibition of the cell cycle or the Ca^{2+}/CaM/CaMK-dependent PASMC proliferation and, ultimately, regression of pulmonary vascular remodelling. It is not known whether halofuginone -mediated improvement of pulmonary haemodynamics (i.e., decreased RVSP and mPAP) may also be due to reduction of cardiac output. Halofuginone is known to inhibit cardiac fibrosis and improve heart function in experimental animals (Huebner et al., 2008; Qin et al., 2017). Further studies are needed to investigate whether halofuginone also reduces VDCC activity and increases K_v channel activity in RV cardiomyocytes, thereby reducing cardiac output.

The in vitro and ex vivo experiments seemed to indicate that halofuginone affects, directly or indirectly, a number of targets to achieve the beneficial or therapeutic effect on experimental PH. The previously published modes of halofuginone actions include inhibition of TGF-β-mediated Smad3 phosphorylation, inhibition of ProRS activity, inhibition of Th17 cell differentiation and inhibition of collagen type I synthesis (Keller et al., 2012; Nagler et al., 1997; Pines, 2008; Roffe et al., 2010; Sundrud et al., 2009). The observations from this study add more modes of its pharmacological actions: activation of K_v channels (e.g., KCNA5), inhibition of Ca^{2+} influx through VDCC, ROCC and SOCC and inhibition of the PI3K/Akt/mTOR signalling pathway in PASMCs. All these actions of halofuginone may contribute to the therapeutic effect on experimental PH shown in this study.

As mentioned earlier, halofuginone is an FDA-approved oral drug for the treatment of scleroderma based on its inhibitory effect on collagen type I synthesis (Pines et al., 2003). Given that collagen deposition in the extracellular matrix contributes to increasing pulmonary vascular wall stiffness and the association of scleroderma with PAH (40% patients with scleroderma develop PAH) (Kolstad et al., 2018), more clinical studies are needed to confirm its beneficial effect on patients with PAH (including associated PAH in patients with scleroderma) and PH due to lung diseases and/or hypoxia.

In conclusion, halofuginone, an FDA-approved low MW drug, is a potent and reversible pulmonary vasodilator and reversed established PH in animals. The mechanisms involved in the acute vasodilator effect and chronic anti-proliferative effect of halofuginone include (i)

activation of K_v channels and enhancement of whole-cell K^+ currents through K_v channels; (ii) inhibition of Ca^{2+} influx through VDCC, ROCC and SOCC; and (iii) inhibition of the PI3K/Akt/mTOR signalling pathway. Taken together with its anti-fibrotic, anti-inflammatory and anti-collagen synthesis effects, halofuginone is potentially a novel and efficient drug for treatment of PAH and PH associated with lung diseases and/or hypoxia and connective tissue disease.

ACKNOWLEDGEMENTS

This study is supported in part by grants from the National Heart, Lung, and Blood Institute of the National Institutes of Health (R35 HL135807, R01 HL146764 and R01 HL142214). A.B. was supported by the American Heart Association Postdoctoral Fellowship (20POST35210959).

DATA AVAILABILITY STATEMENT

Data are available on request from the authors.

Abbreviations:

$[Ca^{2+}]_{cyt}$	cytosolic free Ca^{2+} concentration
AAR	amino acid response
AVD	apoptotic volume decrease
CaM	Ca^{2+}/calmodulin
CaSR	calcium-sensing receptor
CPA	cyclopiazonic acid
DHEA	dehydroepiandrosterone
HPH	hypoxia-induced pulmonary hypertension
HPV	hypoxic pulmonary vasoconstriction
K_{Ca}	Ca^{2+}-activated K^+ channel
K_v	voltage-gated K^+ channel
LV	left ventricle
mPAP	mean pulmonary arterial pressure
mSAP	mean systemic arterial pressure
PA	pulmonary artery
PAH	pulmonary arterial hypertension
PAP	pulmonary artery pressure
PASMCs	pulmonary artery smooth muscle cells

PH	pulmonary hypertension
ProRS	prolyl-tRNA synthetase
PSS	physiological salt solution
ROCC	receptor-operated Ca^{2+} channel
ROCE	receptor-operated Ca^{2+} entry
RV- ± dP/dt	right ventricular contractility
RV	right ventricular
RV/(LV + S)	ratio of the weight of the right ventricle to the weight of the left ventricle and septum (also referred to as Fulton index)
RVP	right ventricular pressure
RVSP	right ventricular systolic pressure
S	septum
sGC	soluble guanylate cyclase
SOCC	store-operated Ca^{2+} channel
SOCE	store-operated Ca^{2+} entry
SR	sarcoplasmic reticulum
VDCC	voltage-dependent Ca^{2+} channel

REFERENCES

Abud EM, Maylor J, Undem C, Punjabi A, Zaiman AL, Myers AC, Sylvester JT, Semenza GL, & Shimoda LA (2012). Digoxin inhibits development of hypoxic pulmonary hypertension in mice. Proceedings of the National Academy of Sciences of the United States of America, 109, 1239–1244. 10.1073/pnas.1120385109 [PubMed: 22232678]

Alexander SPH, Christopoulos A, Davenport AP, Kelly E, Mathie A, Peters JA, Veale EL, Armstrong JF, Faccenda E, Harding SD, Pawson AJ, Sharman JL, Southan C, Davies JA, & CGTP Collaborators. (2019). The Concise Guide to PHARMACOLOGY 2019/20: G protein-coupled receptors. British Journal of Pharmacology, 176, S21–S141. 10.1111/bph.14748 [PubMed: 31710717]

Alexander SPH, Fabbro D, Kelly E, Mathie A, Peters JA, Veale EL, Armstrong JF, Faccenda E, Harding SD, Pawson AJ, Sharman JL, Southan C, Davies JA, & CGTP Collaborators. (2019). The Concise Guide to PHARMACOLOGY 2019/20: Enzymes. British Journal of Pharmacology, 176(Suppl 1), S297–S396. [PubMed: 31710714]

Alexander SPH, Kelly E, Mathie A, Peters JA, Veale EL, Armstrong JF, Faccenda E, Harding SD, Pawson AJ, Sharman JL, Southan C, Davies JA, & CGTP Collaborators. (2019b). The Concise Guide to PHARMACOLOGY 2019/20: Transporters. British Journal of Pharmacology, 176, S397–S493. 10.1111/bph.14753 [PubMed: 31710713]

Alexander SPH, Kelly E, Mathie A, Peters JA, Veale EL, Faccenda E, Harding SD, Pawson AJ, Sharman JL, Southan C, Buneman OP, Cidlowski JA, Christopoulos A, Davenport AP, Fabbro D, Spedding M, Striessnig J, Davies JA, & CGTP Collaborators. (2019a). The Concise Guide

to PHARMACOLOGY 2019/20: Other Protein Targets. British Journal of Pharmacology, 176, S1–S20. 10.1111/bph.14747 [PubMed: 31710719]

Alexander SPH, Mathie A, Peters JA, Veale EL, Striessnig J, Kelly E, Armstrong JF, Faccenda E, Harding SD, Pawson AJ, Sharman JL, Southan C, Davies JA, & CGTP Collaborators. (2019). The Concise Guide to PHARMACOLOGY 2019/20: Ion channels. British Journal of Pharmacology, 176(Suppl 1), S142–S228. [PubMed: 31710715]

Alexander SPH, Roberts RE, Broughton BRS, Sobey CG, George CH, Stanford SC, Cirino G, Docherty JR, Giembycz MA, Hoyer D, Insel PA, Izzo AA, Ji Y, MacEwan DJ, Mangum J, Wonnacott S, & Ahluwalia A (2018). Goals and practicalities of immunoblotting and immunohistochemistry: A guide for submission to the British Journal of Pharmacology. British Journal of Pharmacology, 175, 407–411. 10.1111/bph.14112 [PubMed: 29350411]

Alzoubi A, Toba M, Abe K, O'Neill KD, Rocic P, Fagan KA, McMurtry IF, & Oka M (2013). Dehydroepiandrosterone restores right ventricular structure and function in rats with severe pulmonary arterial hypertension. American Journal of Physiology. Heart and Circulatory Physiology, 304, H1708–H1718. 10.1152/ajpheart.00746.2012 [PubMed: 23585128]

Archer SL, Huang J, Henry T, Peterson D, & Weir EK (1993). A redox-based O_2 sensor in rat pulmonary vasculature. Circulation Research, 73, 1100–1112. 10.1161/01.RES.73.6.1100 [PubMed: 8222081]

Archer SL, Weir EK, Reeve HL, & Michelakis E (2000). Molecular identification of O_2 sensors and O_2-sensitive potassium channels in the pulmonary circulation. Advances in Experimental Medicine and Biology, 475, 219–240. 10.1007/0-306-46825-5_21 [PubMed: 10849663]

Berridge MJ (1995). Calcium signalling and cell proliferation. BioEssays, 17, 491–500. 10.1002/bies.950170605 [PubMed: 7575490]

Bodanovsky A, Guttman N, Barzilai-Tutsch H, Genin O, Levy O, Pines M, & Halevy O (2014). Halofuginone improves muscle-cell survival in muscular dystrophies. Biochimica et Biophysica Acta, 1843, 1339–1347. 10.1016/j.bbamcr.2014.03.025 [PubMed: 24703880]

Bonnet S, Michelakis ED, Porter CJ, Andrade-Navarro MA, Thebaud B, Bonnet S, Haromy A, Harry G, Moudgil R, McMurtry MS, Weir EK, & Archer SL (2006). An abnormal mitochondrial-hypoxia inducible factor-1α–Kv channel pathway disrupts oxygen sensing and triggers pulmonary arterial hypertension in fawn hooded rats: Similarities to human pulmonary arterial hypertension. Circulation, 113, 2630–2641. 10.1161/CIRCULATIONAHA.105.609008 [PubMed: 16735674]

Bouschet T, Martin S, & Henley JM (2008). Regulation of calcium-sensing-receptor trafficking and cell-surface expression by GPCRs and RAMPs. Trends in Pharmacological Sciences, 29, 633–639. 10.1016/j.tips.2008.09.002 [PubMed: 18930324]

Chemla D, Castelain V, Humbert M, Hebert JL, Simonneau G, Lecarpentier Y, & Herve P (2004). New formula for predicting mean pulmonary artery pressure using systolic pulmonary artery pressure. Chest, 126, 1313–1317. 10.1378/chest.126.4.1313 [PubMed: 15486398]

Chen GQ, Tang CF, Shi XK, Lin CY, Fatima S, Pan XH, Yang DJ, Zhang G, Lu AP, Lin SH, & Bian ZX (2015). Halofuginone inhibits colorectal cancer growth through suppression of Akt/mTORC1 signaling and glucose metabolism. Oncotarget, 6, 24148–24162. 10.18632/oncotarget.4376 [PubMed: 26160839]

Chu TL, Guan Q, Nguan CY, & Du C (2013). Halofuginone suppresses T cell proliferation by blocking proline uptake and inducing cell apoptosis. International Immunopharmacology, 16, 414–423. 10.1016/j.intimp.2013.04.031 [PubMed: 23685128]

Curtis MJ, Bond RA, Spina D, Ahluwalia A, Alexander SP, Giembycz MA, Gilchrist A, Hoyer D, Insel PA, Izzo AA, Lawrence AJ, MacEwan DJ, Moon LDF, Wonnacott S, Weston AH, & McGrath JC (2015). Experimental design and analysis and their reporting: New guidance for publication in BJP. British Journal of Pharmacology, 172, 3461–3471. 10.1111/bph.12856 [PubMed: 26114403]

de Figueiredo-Pontes LL, Assis PA, Santana-Lemos BA, Jacomo RH, Lima AS, Garcia AB, Thomé CH, Araújo AG, Panepucci RA, Zago MA, Nagler A, Falcão RP, & Rego EM (2011). Halofuginone has anti-proliferative effects in acute promyelocytic leukemia by modulating the transforming growth factor beta signaling pathway. PLoS One, 6(10), e26713. [PubMed: 22053203]

Elkin M, Ariel I, Miao HQ, Nagler A, Pines M, de-Groot N, Hochberg A, & Vlodavsky I (1999). Inhibition of bladder carcinoma angiogenesis, stromal support, and tumor growth by halofuginone. Cancer Research, 59, 4111–4118. [PubMed: 10463616]

Elkin M, Miao HQ, Nagler A, Aingorn E, Reich R, Hemo I, Dou HL, Pines M, & Vlodavsky I (2000). Halofuginone: A potent inhibitor of critical steps in angiogenesis progression. The FASEB Journal, 14, 2477–2485. 10.1096/fj.00-0292com [PubMed: 11099465]

Fleischmann BK, Murray RK, & Kotlikoff MI (1994). Voltage window for sustained elevation of cytosolic calcium in smooth muscle cells. Proceedings of the National Academy of Sciences of the United States of America, 91, 11914–11918. 10.1073/pnas.91.25.11914 [PubMed: 7527547]

Follo C, Vidoni C, Morani F, Ferraresi A, Seca C, & Isidoro C (2019). Amino acid response by Halofuginone in Cancer cells triggers autophagy through proteasome degradation of mTOR. Cell Communication and Signaling: CCS, 17(1), 39. 10.1186/s12964-019-0354-2 [PubMed: 31046771]

Galie N, Humbert M, Vachiery JL, Gibbs S, Lang I, Torbicki A, Simonneau G, Peacock A, Vonk Noordegraaf A, Beghetti M, Ghofrani A, Gomez Sanchez MA, Hansmann G, Klepetko W, Lancellotti P, Matucci M, McDonagh T, Pierard LA, Trindade PT, … ESC Scientific Document Group. (2015). ESC/ERS guidelines for the diagnosis and treatment of pulmonary hypertension: The Joint Task Force for the Diagnosis and Treatment of Pulmonary Hypertension of the European Society of Cardiology (ESC) and the European Respiratory Society (ERS): Endorsed by: Association for European Paediatric and Congenital Cardiology (AEPC), International Society for Heart and Lung Transplantation (ISHLT). The European Respiratory Journal, 46, 903–975. [PubMed: 26318161]

Gnainsky Y, Kushnirsky Z, Bilu G, Hagai Y, Genina O, Volpin H, Bruck R, Spira G, Nagler A, Kawada N, Yoshizato K, Reinhardt DP, Libermann TA, & Pines M (2007). Gene expression during chemically induced liver fibrosis: Effect of halofuginone on TGF-β signaling. Cell and Tissue Research, 328, 153–166. 10.1007/s00441-006-0330-1 [PubMed: 17180598]

Gnainsky Y, Spira G, Paizi M, Bruck R, Nagler A, Abu-Amara SN, Geiger B, Genina O, Monsonego-Ornan E, & Pines M (2004). Halofuginone, an inhibitor of collagen synthesis by rat stellate cells, stimulates insulin-like growth factor binding protein-1 synthesis by hepatocytes. Journal of Hepatology, 40, 269–277. 10.1016/j.jhep.2003.10.020 [PubMed: 14739098]

Golovina VA, Platoshyn O, Bailey CL, Wang J, Limsuwan A, Sweeney M, Rubin LJ, & Yuan JXJ (2001). Upregulated TRP and enhanced capacitative Ca^{2+} entry in human pulmonary artery myocytes during proliferation. American Journal of Physiology. Heart and Circulatory Physiology, 280, H746–H755. 10.1152/ajpheart.2001.280.2.H746 [PubMed: 11158974]

Goncharov DA, Kudryashova TV, Ziai H, Ihida-Stansbury K, DeLisser H, Krymskaya VP, Tuder RM, Kawut SM, & Goncharova EA (2014). Mammalian target of rapamycin complex 2 (mTORC2) coordinates pulmonary artery smooth muscle cell metabolism, proliferation, and survival in pulmonary arterial hypertension. Circulation, 129, 864–874. 10.1161/CIRCULATIONAHA.113.004581 [PubMed: 24270265]

Graef IA, Chen F, Chen L, Kuo A, & Crabtree GR (2001). Signals transduced by Ca^{2+}/calcineurin and NFATc3/c4 pattern the developing vasculature. Cell, 105, 863–875. 10.1016/S0092-8674(01)00396-8 [PubMed: 11439183]

Grudzien MM, Low PS, Manning PC, Arredondo M, Belton RJ Jr., & Nowak RA (2010). The antifibrotic drug halofuginone inhibits proliferation and collagen production by human leiomyoma and myometrial smooth muscle cells. Fertility and Sterility, 93, 1290–1298. 10.1016/j.fertnstert.2008.11.018 [PubMed: 19135664]

Hirenallur SD, Haworth ST, Leming JT, Chang J, Hernandez G, Gordon JB, & Rusch NJ (2008). Upregulation of vascular calcium channels in neonatal piglets with hypoxia-induced pulmonary hypertension. American Journal of Physiology. Lung Cellular and Molecular Physiology, 295, L915–L924. 10.1152/ajplung.90286.2008 [PubMed: 18776054]

Hoeper MM, Barst RJ, Bourge RC, Feldman J, Frost AE, Galie N, Gómez-Sánchez MA, Grimminger F, Grünig E, Hassoun PM, Morrell NW, Peacock AJ, Satoh T, Simonneau G, Tapson VF, Torres F, Lawrence D, Quinn DA, & Ghofrani H-A (2013). Imatinib mesylate as add-on therapy for pulmonary arterial hypertension: Results of the randomized IMPRES study. Circulation, 127, 1128–1138. 10.1161/CIRCULATIONAHA.112.000765 [PubMed: 23403476]

Houssaini A, Abid S, Mouraret N, Wan F, Rideau D, Saker M, Marcos E, Tissot CM, Dubois-Randé JL, Amsellem V, & Adnot S (2013). Rapamycin reverses pulmonary artery smooth muscle cell proliferation in pulmonary hypertension. American Journal of Respiratory Cell and Molecular Biology, 48, 568–577. 10.1165/rcmb.2012-0429OC [PubMed: 23470622]

Huebner KD, Jassal DS, Halevy O, Pines M, & Anderson JE (2008). Functional resolution of fibrosis in *mdx* mouse dystrophic heart and skeletal muscle by halofuginone. American Journal of Physiology. Heart and Circulatory Physiology, 294, H1550–H1561. [PubMed: 18263710]

Jain PP, Hosokawa S, Xiong M, Babicheva A, Zhao T, Rodriguez M, Rahimi S, Pourhashemi K, Balistrieri F, Lai N, Malhotra A, Shyy JY-J, Valdez-Jasso D, Thistlethwaite PA, Makino A, & Yuan JX-J (2020). Revisiting the mechanism of hypoxic pulmonary vasoconstriction using isolated perfused/ventilated mouse lung. Pulmonary Circulation, 10(4), 1–18.

Jiang S, Zeng Q, Gettayacamin M, Tungtaeng A, Wannaying S, Lim A, Hansukjariya P, Okunji CO, Zhu S, & Fang D (2005). Antimalarial activities and therapeutic properties of febrifugine analogs. Antimicrobial Agents and Chemotherapy, 49, 1169–1176. 10.1128/AAC.49.3.1169-1176.2005 [PubMed: 15728920]

Jin ML, Park SY, Kim YH, Park G, & Lee SJ (2014). Halofuginone induces the apoptosis of breast cancer cells and inhibits migration via downregulation of matrix metalloproteinase-9. International Journal of Oncology, 44, 309–318. 10.3892/ijo.2013.2157 [PubMed: 24173318]

Juarez P, Fournier PGJ, Mohammad KS, McKenna RC, Davis HW, Peng XH, Niewolna M, Mauviel A, Chirgwin JM, & Guise TA (2017). Halofuginone inhibits TGF-β/BMP signaling and in combination with zoledronic acid enhances inhibition of breast cancer bone metastasis. Oncotarget, 8, 86447–86462. 10.18632/oncotarget.21200 [PubMed: 29156807]

Juarez P, Mohammad KS, Yin JJ, Fournier PG, McKenna RC, Davis HW, Peng XH, Niewolna M, Javelaud D, Chirgwin JM, Mauviel A, & Guise TA (2012). Halofuginone inhibits the establishment and progression of melanoma bone metastases. Cancer Research, 72, 6247–6256. 10.1158/0008-5472.CAN-12-1444 [PubMed: 23002206]

Kahl CR, & Means AR (2003). Regulation of cell cycle progression by calcium/calmodulin-dependent pathways. Endocrine Reviews, 24, 719–736. 10.1210/er.2003-0008 [PubMed: 14671000]

Keller TL, Zocco D, Sundrud MS, Hendrick M, Edenius M, Yum J, Kim YJ, Lee HK, Cortese JF, Wirth DF, Dignam JD, Rao A, Yeo CY, Mazitschek R, & Whitman M (2012). Halofuginone and other febrifugine derivatives inhibit prolyl-tRNA synthetase. Nature Chemical Biology, 8, 311–317. 10.1038/nchembio.790 [PubMed: 22327401]

Koepfli JB, Mead JF, & Brockman JA Jr. (1947). An alkaloid with high antimalarial activity from *Dichroa febrifuga*. Journal of the American Chemical Society, 69(7), 1837. 10.1021/ja01199a513 [PubMed: 20251439]

Kolstad KD, Li S, Steen V, Chung L, & Investigators P (2018). Long-term outcomes in systemic sclerosis-associated pulmonary arterial hypertension from the Pulmonary Hypertension Assessment and Recognition of Outcomes in Scleroderma Registry (PHAROS). Chest, 154, 862–871. 10.1016/j.chest.2018.05.002 [PubMed: 29777655]

Krick S, Platoshyn O, Sweeney M, McDaniel SS, Zhang S, Rubin LJ, & Yuan JX-J (2002). Nitric oxide induces apoptosis by activating K^+ channels in pulmonary vascular smooth muscle cells. American Journal of Physiology. Heart and Circulatory Physiology, 282, H184–H193. 10.1152/ajpheart.2002.282.1.H184 [PubMed: 11748062]

Kudryashova TV, Goncharov DA, Pena A, Ihida-Stansbury K, DeLisser H, Kawut SM, & Goncharova EA (2015). Profiling the role of mammalian target of rapamycin in the vascular smooth muscle metabolome in pulmonary arterial hypertension. Pulmonary Circulation, 5, 667–680. 10.1086/683810 [PubMed: 26697174]

Kuga T, Kobayashi S, Hirakawa Y, Kanaide H, & Takeshita A (1996). Cell cycle-dependent expression of L- and T-type Ca^{2+} currents in rat aortic smooth muscle cells in primary culture. Circulation Research, 79, 14–19. 10.1161/01.RES.79.1.14 [PubMed: 8925562]

Kuhr FK, Smith KA, Song MY, Levitan I, & Yuan JX (2012). New mechanisms of pulmonary arterial hypertension: Role of Ca^{2+} signaling. American Journal of Physiology. Heart and Circulatory Physiology, 302, H1546–H1562. 10.1152/ajpheart.00944.2011 [PubMed: 22245772]

Kunimi H, Miwa Y, Inoue H, Tsubota K, & Kurihara T (2019). A novel HIF inhibitor halofuginone prevents neurodegeneration in a murine model of retinal ischemia-reperfusion. International Journal of Molecular Sciences, 20(13), 3171. 10.3390/ijms20133171 [PubMed: 31261724]

Leiba M, Cahalon L, Shimoni A, Lider O, Zanin-Zhorov A, Hecht I, Sela U, Vlodavsky I, & Nagler A (2006). Halofuginone inhibits NF-κB and p38 MAPK in activated T cells. Journal of Leukocyte Biology, 80, 399–406. 10.1189/jlb.0705409 [PubMed: 16769768]

Levi-Schaffer F, Nagler A, Slavin S, Knopov V, & Pines M (1996). Inhibition of collagen synthesis and changes in skin morphology in murine graft-versus-host disease and tight skin mice: Effect of halofuginone. The Journal of Investigative Dermatology, 106, 84–88. 10.1111/1523-1747.ep12328014 [PubMed: 8592087]

Lilley E, Stanford SC, Kendall DE, Alexander SP, Cirino G, Docherty JR, George CH, Insel PA, Izzo AA, Ji Y, Panettieri RA, Sobey CG, Stefanska B, Stephens G, Teixeira M, & Ahluwalia A (2020). ARRIVE 2.0 and the British Journal of Pharmacology: Updated guidance for 2020. British Journal of Pharmacology, 177(16), 3611–3616. 10.1111/bph.15178 [PubMed: 32662875]

Lin MJ, Leung GP, Zhang WM, Yang XR, Yip KP, Tse CM, & Sham JS (2004). Chronic hypoxia-induced upregulation of store-operated and receptor-operated Ca^{2+} channels in pulmonary arterial smooth muscle cells: A novel mechanism of hypoxic pulmonary hypertension. Circulation Research, 95, 496–505. 10.1161/01.RES.0000138952.16382.ad [PubMed: 15256480]

Lindegaard Pedersen M, Kruger M, Grimm D, Infanger M, & Wehland M (2019). The prostacyclin analogue treprostinil in the treatment of pulmonary arterial hypertension. Basic & Clinical Pharmacology & Toxicology, 126, 32–42. 10.1111/bcpt.13305

Liu XR, Zhang MF, Yang N, Liu Q, Wang RX, Cao YN, Yang XR, Sham JSK, & Lin MJ (2012). Enhanced store-operated Ca^{2+} entry and TRPC channel expression in pulmonary arteries of monocrotaline-induced pulmonary hypertensive rats. American Journal of Physiology. Cell Physiology, 302, C77–C87. 10.1152/ajpcell.00247.2011 [PubMed: 21940663]

MacLean MMR (2018). The serotonin hypothesis in pulmonary hypertension revisited: Targets for novel therapies (2017 Grover Conference Series). Pulmonary Circulation, 8(2), 1–9.

Magno AL, Ward BK, & Ratajczak T (2011). The calcium-sensing receptor: A molecular perspective. Endocrine Reviews, 32, 3–30. 10.1210/er.2009-0043 [PubMed: 20729338]

McDaniel SS, Platoshyn O, Wang J, Yu Y, Sweeney M, Krick S, Rubin LJ, & Yuan JX (2001). Capacitative Ca^{2+} entry in agonist-induced pulmonary vasoconstriction. American Journal of Physiology. Lung Cellular and Molecular Physiology, 280, L870–L880. 10.1152/ajplung.2001.280.5.L870 [PubMed: 11290510]

Nagler A, Firman N, Feferman R, Cotev S, Pines M, & Shoshan S (1996). Reduction in pulmonary fibrosis in vivo by halofuginone. American Journal of Respiratory and Critical Care Medicine, 154, 1082–1086. 10.1164/ajrccm.154.4.8887611 [PubMed: 8887611]

Nagler A, Genina O, Lavelin I, Ohana M, & Pines M (1999). Halofuginone, an inhibitor of collagen type I synthesis, prevents postoperative adhesion formation in the rat uterine horn model. American Journal of Obstetrics and Gynecology, 180, 558–563. 10.1016/S0002-9378(99)70254-1 [PubMed: 10076128]

Nagler A, Gofrit O, Ohana M, Pode D, Genina O, & Pines M (2000). The effect of halofuginone, an inhibitor of collagen type I synthesis, on urethral stricture formation: In vivo and in vitro study in a rat model. The Journal of Urology, 164, 1776–1780. 10.1016/S0022-5347(05)67105-4 [PubMed: 11025768]

Nagler A, Miao HQ, Aingorn H, Pines M, Genina O, & Vlodavsky I (1997). Inhibition of collagen synthesis, smooth muscle cell proliferation, and injury-induced intimal hyperplasia by halofuginone. Arteriosclerosis, Thrombosis, and Vascular Biology, 17, 194–202. 10.1161/01.ATV.17.1.194 [PubMed: 9012656]

Nagler A, Rivkind AI, Raphael J, Levi-Schaffer F, Genina O, Lavelin I, & Pines M (1998). Halofuginone–an inhibitor of collagen type I synthesis–prevents postoperative formation of abdominal adhesions. Annals of Surgery, 227, 575–582. 10.1097/00000658-199804000-00021 [PubMed: 9563549]

Nelson EF, Huang CW, Ewel JM, Chang AA, & Yuan C (2012). Halofuginone down-regulates Smad3 expression and inhibits the TGFbeta-induced expression of fibrotic markers in human corneal fibroblasts. Molecular Vision, 18, 479–487. [PubMed: 22393274]

Nelson MT, & Quayle JM (1995). Physiological roles and properties of potassium channels in arterial smooth muscle. The American Journal of Physiology, 268, C799–C822. 10.1152/ajpcell.1995.268.4.C799 [PubMed: 7733230]

Parasuraman S, Walker S, Loudon BL, Gollop ND, Wilson AM, Lowery C, & Frenneaux MP (2016). Assessment of pulmonary artery pressure by echocardiography–A comprehensive review. International Journal of Cardiology Heart & Vasculature, 12, 45–51. 10.1016/j.ijcha.2016.05.011 [PubMed: 28616542]

Park MK, Park JS, Park EM, Lim MA, Kim SM, Lee DG, Baek SY, Yang EJ, Woo JW, Lee J, Kwok SK, Kim HY, Cho ML, & Park SH (2014). Halofuginone ameliorates autoimmune arthritis in mice by regulating the balance between Th17 and Treg cells and inhibiting osteoclastogenesis. Arthritis & Rhematology, 66, 1195–1207. 10.1002/art.38313

Paulin R, Meloche J, Jacob MH, Bisserier M, Courboulin A, & Bonnet S (2011). Dehydroepiandrosterone inhibits the Src/STAT3 constitutive activation in pulmonary arterial hypertension. American Journal of Physiology. Heart and Circulatory Physiology, 301, H1798–H1809. 10.1152/ajpheart.00654.2011 [PubMed: 21890685]

Percie du Sert N, Hurst V, Ahluwalia A, Alam S, Avey MT, Baker M, Browne WJ, Clark A, Cuthill IC, Dirnagl U, Emerson M, Garner P, Holgate ST, Howells DW, Karp NA, Lazic SE, Lidster K, MacCallum CJ, Macleod M, … Würbel H (2020). The ARRIVE guidelines 2.0: Updated guidelines for reporting animal research. PLoS Biology, 18(7), e3000410. 10.1371/journal.pbio.3000410 [PubMed: 32663219]

Pines M (2008). Targeting TGFβ signaling to inhibit fibroblast activation as a therapy for fibrosis and cancer: Effect of halofuginone. Expert Opinion on Drug Discovery, 3, 11–20. 10.1517/17460441.3.1.11 [PubMed: 23480137]

Pines M (2014). Halofuginone for fibrosis, regeneration and cancer in the gastrointestinal tract. World Journal of Gastroenterology, 20, 14778–14786. 10.3748/wjg.v20.i40.14778 [PubMed: 25356039]

Pines M, Domb A, Ohana M, Inbar J, Genina O, Alexiev R, & Nagler A (2001). Reduction in dermal fibrosis in the tight-skin (Tsk) mouse after local application of halofuginone. Biochemical Pharmacology, 62, 1221–1227. 10.1016/S0006-2952(01)00753-5 [PubMed: 11705455]

Pines M, Snyder D, Yarkoni S, & Nagler A (2003). Halofuginone to treat fibrosis in chronic graft-versus-host disease and scleroderma. Biology of Blood and Marrow Transplantation, 9, 417–425. 10.1016/S1083-8791(03)00151-4 [PubMed: 12869955]

Pines M, & Spector I (2015). Halofuginone–The multifaceted molecule. Molecules, 20, 573–594. 10.3390/molecules20010573 [PubMed: 25569515]

Platoshyn O, Brevnova EE, Burg ED, Yu Y, Remillard CV, & Yuan JX (2006). Acute hypoxia selectively inhibits KCNA5 channels in pulmonary artery smooth muscle cells. American Journal of Physiology. Cell Physiology, 290, C907–C916. 10.1152/ajpcell.00028.2005 [PubMed: 16236819]

Popov Y, Patsenker E, Bauer M, Niedobitek E, Schulze-Krebs A, & Schuppan D (2006). Halofuginone induces matrix metalloproteinases in rat hepatic stellate cells via activation of p38 and NFκB. The Journal of Biological Chemistry, 281, 15090–15098. 10.1074/jbc.M600030200 [PubMed: 16489207]

Post JM, Gelband CH, & Hume JR (1995). $[Ca^{2+}]_i$ inhibition of K^+ channels in canine pulmonary artery: Novel mechanism for hypoxia-induced membrane depolarization. Circulation Research, 77, 131–139. 10.1161/01.RES.77.1.131 [PubMed: 7788871]

Prins KW, Thenappan T, Weir EK, Kalra R, Pritzker M, & Archer SL (2019). Repurposing medications for treatment of pulmonary arterial hypertension: What's old is new again. Journal of the American Heart Association, 8, e011343. [PubMed: 30590974]

Qin P, Arabacilar P, Bernard RE, Bao W, Olzinski AR, Guo Y, Lal H, Eisennagel SH, Platchek MC, Xie W, del Rosario J, Nayal M, Lu Q, Roethke T, Schnackenberg CG, Wright F, Quaile MP, Halsey WS, Hughes AM, … Willette RN (2017). Activation of the amino acid response pathway blunts the effects of cardiac stress. Journal of the American Heart Association, 6, e004453. 10.1161/JAHA.116.004453 [PubMed: 28487390]

Quatredeniers M, Nakhleh MK, Dumas SJ, Courboulin A, Vinhas MC, Antigny F, Phan C, Guignabert C, Bendifallah I, Vocelle M, Fadel E, Dorfmüller P, Humbert M, & Cohen-Kaminsky S (2019). Functional interaction between PDGFβ and GluN2B-containing NMDA receptors in

smooth muscle cell proliferation and migration in pulmonary arterial hypertension. American Journal of Physiology. Lung Cellular and Molecular Physiology, 316, L445–L455. 10.1152/ajplung.00537.2017 [PubMed: 30543306]

Rieg AD, Suleiman S, Anker C, Verjans E, Rossaint R, Uhlig S, & Martin C (2018). PDGF-BB regulates the pulmonary vascular tone: Impact of prostaglandins, calcium, MAPK- and PI3K/AKT/mTOR signalling and actin polymerisation in pulmonary veins of guinea pigs. Respiratory Research, 19, 120. 10.1186/s12931-018-0829-5 [PubMed: 29921306]

Roffe S, Hagai Y, Pines M, & Halevy O (2010). Halofuginone inhibits Smad3 phosphorylation via the PI3K/Akt and MAPK/ERK pathways in muscle cells: Effect on myotube fusion. Experimental Cell Research, 316, 1061–1069. 10.1016/j.yexcr.2010.01.003 [PubMed: 20060825]

Rothman AMK, Vachiery JL, Howard LS, Mikhail GW, Lang IM, Jonas M, Kiely DG, Shav D, Shabtay O, Avriel A, Lewis GD, Rosenzweig EB, Kirtane AJ, Kim NH, Mahmud E, McLaughlain VV, Chetcuti S, Leon MB, Ben-Yehuda O, & Rubin LJ (2020). Intravascular ultrasound pulmonary artery denervation to treat pulmonary arterial hypertension (TROPHY1): Multicenter, early feasibility study. JACC Cardiovascular Interventions, 13, 989–999. 10.1016/j.jcin.2019.12.027 [PubMed: 32327095]

Sakao S, Voelkel NF, Tanabe N, & Tatsumi K (2015). Determinants of an elevated pulmonary arterial pressure in patients with pulmonary arterial hypertension. Respiratory Research, 16, 84. 10.1186/s12931-015-0246-y [PubMed: 26150101]

Samant BS, & Sukhthankar MG (2009). Synthesis and comparison of antimalarial activity of febrifugine derivatives including halofuginone. Medicinal Chemistry, 5, 293–300. [PubMed: 19442220]

Seidler NW, Jona I, Vegh M, & Martonosi A (1989). Cyclopiazonic acid is a specific inhibitor of the Ca^{2+}-ATPase of sarcoplasmic reticulum. The Journal of Biological Chemistry, 264, 17816–17823. 10.1016/S0021-9258(19)84646-X [PubMed: 2530215]

Shang F, Zhang J, Li Z, Zhang J, Yin Y, Wang Y, Marin TL, Gongol B, Xiao H, Zhang YY, Chen Z, Shyy JYJ, & Lei T (2016). Cardiovascular protective effect of metformin and telmisartan: Reduction of PARP1 activity via the AMPK-PARP1 cascade. PLoS One, 11, e0151845. 10.1371/journal.pone.0151845 [PubMed: 26986624]

Sheffer Y, Leon O, Pinthus JH, Nagler A, Mor Y, Genin O, Iluz M, Kawada N, Yoshizato K, & Pines M (2007). Inhibition of fibroblast to myofibroblast transition by halofuginone contributes to the chemotherapy-mediated antitumoral effect. Molecular Cancer Therapeutics, 6, 570–577. 10.1158/1535-7163.MCT-06-0468 [PubMed: 17267660]

Sheng M, McFadden G, & Greenberg ME (1990). Membrane depolarization and calcium induce *c-fos* transcription via phosphorylation of transcription factor CREB. Neuron, 4, 571–582. 10.1016/0896-6273(90)90115-V [PubMed: 2157471]

Simonneau G, Montani D, Celermajer DS, Denton CP, Gatzoulis MA, Krowka M, Williams PG, & Souza R (2019). Haemodynamic definitions and updated clinical classification of pulmonary hypertension. The European Respiratory Journal, 53, 1801913. 10.1183/13993003.01913-2018 [PubMed: 30545968]

Smith KA, Voiriot G, Tang H, Fraidenburg DR, Song S, Yamamura H, Yamamura A, Guo Q, Wan J, Pohl NM, Tauseef M, Bodmer R, Ocorr K, Thistlethwaite PA, Haddad GG, Powell FL, Makino A, Mehta D, & Yuan JXJ (2015). Notch activation of Ca^{2+} signaling in the development of hypoxic pulmonary vasoconstriction and pulmonary hypertension. American Journal of Respiratory Cell and Molecular Biology, 53, 355–367. 10.1165/rcmb.2014-0235OC [PubMed: 25569851]

Song MY, Makino A, & Yuan JX (2011). STIM2 contributes to enhanced store-operated Ca^{2+} entry in pulmonary artery smooth muscle cells from patients with idiopathic pulmonary arterial hypertension. Pulmonary Circulation, 1, 84–94. 10.4103/2045-8932.78106 [PubMed: 21709766]

Song S, Babicheva A, Zhao T, Ayon RJ, Rodriguez M, Rahimi S, Balistrieri F, Harrington A, Shyy JYJ, Thistlethwaite PA, Makino A, & Yuan JXJ (2020). Notch enhances Ca^{2+} entry by activating calcium-sensing receptors and inhibiting voltage-gated K^+ channels. American Journal of Physiology. Cell Physiology, 318, C954–C968. 10.1152/ajpcell.00487.2019 [PubMed: 32186932]

Song S, Jacobson KN, McDermott KM, Reddy SP, Cress AE, Tang H, Dudek SM, Black SM, Garcia JG, Makino A, & Yuan JX (2016). ATP promotes cell survival via regulation of cytosolic [Ca^{2+}]

and Bcl-2/Bax ratio in lung cancer cells. American Journal of Physiology. Cell Physiology, 310, C99–C114. 10.1152/ajpcell.00092.2015 [PubMed: 26491047]

Sourbier C, Lindner V, Lang H, Agouni A, Schordan E, Danilin S, Rothhut S, Jacqmin D, Helwig JJ, & Massfelder T (2006). The phosphoinositide 3-kinase/Akt pathway: A new target in human renal cell carcinoma therapy. Cancer Research, 66, 5130–5142. 10.1158/0008-5472.CAN-05-1469 [PubMed: 16707436]

Spector I, Zilberstein Y, Lavy A, Nagler A, Genin O, & Pines M (2012). Involvement of host stroma cells and tissue fibrosis in pancreatic tumor development in transgenic mice. PLoS One, 7, e41833. 10.1371/journal.pone.0041833 [PubMed: 22848627]

Stecklair KP, Hamburger DR, Egorin MJ, Parise RA, Covey JM, & Eiseman JL (2001). Pharmacokinetics and tissue distribution of halofuginone (NSC 713205) in CD2F1 mice and Fischer 344 rats. Cancer Chemotherapy and Pharmacology, 48, 375–382. 10.1007/s002800100367 [PubMed: 11761455]

Stenmark KR, Meyrick B, Galie N, Mooi WJ, & McMurtry IF (2009). Animal models of pulmonary arterial hypertension: The hope for etiological discovery and pharmacological cure. American Journal of Physiology. Lung Cellular and Molecular Physiology, 297, L1013–L1032. 10.1152/ajplung.00217.2009 [PubMed: 19748998]

Sundrud MS, Koralov SB, Feuerer M, Calado DP, Kozhaya AE, Rhule-Smith A, Lefebvre RE, Unutmaz D, Mazitschek R, Waldner H, Whitman M, Keller T, & Rao A (2009). Halofuginone inhibits TH17 cell differentiation by activating the amino acid starvation response. Science, 324, 1334–1338. 10.1126/science.1172638 [PubMed: 19498172]

Tabima DM, Hacker TA, & Chesler NC (2010). Measuring right ventricular function in the normal and hypertensive mouse hearts using admittance-derived pressure-volume loops. American Journal of Physiology. Heart and Circulatory Physiology, 299, H2069–H2075. 10.1152/ajpheart.00805.2010 [PubMed: 20935149]

Tang H, Chen J, Fraidenburg DR, Song S, Sysol JR, Drennan AR, Offermanns S, Ye RD, Bonini MG, Minshall RD, Garcia JGN, Machado RF, Makino A, & Yuan JXJ (2015). Deficiency of Akt1, but not Akt2, attenuates the development of pulmonary hypertension. American Journal of Physiology. Lung Cellular and Molecular Physiology, 308, L208–L220. 10.1152/ajplung.00242.2014 [PubMed: 25416384]

Tang H, Wu K, Wang J, Vinjamuri S, Gu Y, Song S, Wang Z, Zhang Q, Balistrieri A, Ayon RJ, Rischard F, Vanderpool R, Chen J, Zhou G, Desai AA, Black SM, Garcia JGN, Yuan JXJ, & Makino A (2018). Pathogenic role of mTORC1 and mTORC2 in pulmonary hypertension. JACC Basic to Translational Science, 3, 744–762. 10.1016/j.jacbts.2018.08.009 [PubMed: 30623134]

Tang H, Yamamura A, Yamamura H, Song S, Fraidenburg DR, Chen J, Gu Y, Pohl NM, Zhou T, Jiménez-Pérez L, Ayon RJ, Desai AA, Goltzman D, Rischard F, Khalpey Z, Black SM, Garcia JGN, Makino A, & Yuan JXJ (2016). Pathogenic role of calcium-sensing receptors in the development and progression of pulmonary hypertension. American Journal of Physiology. Lung Cellular and Molecular Physiology, 310, L846–L859. 10.1152/ajplung.00050.2016 [PubMed: 26968768]

Taras D, Blanc JF, Rullier A, Dugot-Senant N, Laurendeau I, Bieche I, Pines M, & Rosenbaum J (2006). Halofuginone suppresses the lung metastasis of chemically induced hepatocellular carcinoma in rats through MMP inhibition. Neoplasia, 8, 312–318. 10.1593/neo.05796 [PubMed: 16756723]

Tuder RM (2017). Pulmonary vascular remodeling in pulmonary hypertension. Cell and Tissue Research, 367, 643–649. 10.1007/s00441-016-2539-y [PubMed: 28025704]

Tuder RM, Archer SL, Dorfmuller P, Erzurum SC, Guignabert C, Michelakis E, Rabinovitch M, Schermuly R, Stenmark KR, & Morrell NW (2013). Relevant issues in the pathology and pathobiology of pulmonary hypertension. Journal of the American College of Cardiology, 62, D4–D12. 10.1016/j.jacc.2013.10.025 [PubMed: 24355640]

Vitali SH, Hansmann G, Rose C, Fernandez-Gonzalez A, Scheid A, Mitsialis SA, & Kourembanas S (2014). The Sugen 5416/hypoxia mouse model of pulmonary hypertension revisited: Long-term follow-up. Pulmonary Circulation, 4, 619–629. 10.1086/678508 [PubMed: 25610598]

Wan J, Yamamura A, Zimnicka AM, Voiriot G, Smith KA, Tang H, Ayon RJ, Choudhury MSR, Ko EA, Wang J, Wang C, Makino A, & Yuan JX-J (2013). Chronic hypoxia seletively enhances L-

and T-type voltage-dependent Ca^{2+} channel activity in pulmonary artery by upregulating $Ca_V1.2$ and $Ca_V3.2$. American Journal of Physiology-Lung Cellular and Molecular Physiology, 305, L154–L164. [PubMed: 23686856]

Wang J, Shimoda LA, Weigand L, Wang W, Sun D, & Sylvester JT (2005). Acute hypoxia increases intracellular [Ca^{2+}] in pulmonary arterial smooth muscle by enhancing capacitative Ca^{2+} entry. American Journal of Physiology. Lung Cellular and Molecular Physiology, 288, L1059–L1069. 10.1152/ajplung.00448.2004 [PubMed: 15665040]

Wang J, Wang B, Lv X, & Wang Y (2020). Halofuginone functions as a therapeutic drug for chronic periodontitis in a mouse model. International Journal of Immunopathology and Pharmacology, 34, 1–9.

Wang J, Weigand L, Lu W, Sylvester JT, Semenza GL, & Shimoda LA (2006). Hypoxia inducible factor 1 mediates hypoxia-induced TRPC expression and elevated intracellular Ca^{2+} in pulmonary arterial smooth muscle cells. Circulation Research, 98, 1528–1537. 10.1161/01.RES.0000227551.68124.98 [PubMed: 16709899]

Weir EK, Obreztchikova M, Vargese A, Cabrera JA, Peterson DA, & Hong Z (2008). Mechanisms of oxygen sensing: A key to therapy of pulmonary hypertension and patent ductus arteriosus. British Journal of Pharmacology, 155, 300–307. 10.1038/bjp.2008.291 [PubMed: 18641675]

Wilkins MR, Ghofrani HA, Weissmann N, Aldashev A, & Zhao L (2015). Pathophysiology and treatment of high-altitude pulmonary vascular disease. Circulation, 131, 582–590. 10.1161/CIRCULATIONAHA.114.006977 [PubMed: 25666980]

Woo SU, Sangai T, Akcakanat A, Chen H, Wei C, & Meric-Bernstam F (2017). Vertical inhibition of the PI3K/Akt/mTOR pathway is synergistic in breast cancer. Oncogene, 6, 1–7. 10.1038/oncsis.2017.86

Wu K, Zhang Q, Wu X, Lu W, Tang H, Liang Z, Gu Y, Song S, Ayon RJ, Wang Z, McDermott KM, Balistrieri A, Wang C, Black SM, Garcia JGN, Makino A, Yuan JXJ, & Wang J (2017). Chloroquine is a potent pulmonary vasodilator that attenuates hypoxia-induced pulmonary hypertension. British Journal of Pharmacology, 174, 4155–4172. 10.1111/bph.13990 [PubMed: 28849593]

Xia Y, Fu Z, Hu J, Huang C, Paudel O, Cai S, Liedtke W, & Sham JSK (2013). TRPV4 channel contributes to serotonin-induced pulmonary vasoconstriction and the enhanced vascular reactivity in chronic hypoxic pulmonary hypertension. American Journal of Physiology. Cell Physiology, 305, C704–C715. 10.1152/ajpcell.00099.2013 [PubMed: 23739180]

Xiao R, Su Y, Feng T, Sun M, Liu B, Zhang J, Lu Y, Li J, Wang T, Zhu L, & Hu Q (2017). Monocrotaline induces endothelial injury and pulmonary hypertension by targeting the extracellular calcium-sensing receptor. Journal of the American Heart Association, 6, e004865. 10.1161/JAHA.116.004865 [PubMed: 28330842]

Xiao Y, Peng H, Hong C, Chen Z, Deng X, Wang A, Yang F, Yang L, Chen C, & Qin X (2017). PDGF promotes the Warburg effect in pulmonary arterial smooth muscle cells via activation of the PI3K/AKT/mTOR/HIF-1α signaling pathway. Cellular Physiology and Biochemistry, 42, 1603–1613. 10.1159/000479401 [PubMed: 28738389]

Xu F, Na L, Li Y, & Chen L (2020). Roles of the PI3K/AKT/mTOR signalling pathways in neurodegenerative diseases and tumours. Cell & Bioscience, 10, 54. 10.1186/s13578-020-00416-0 [PubMed: 32266056]

Yamamura A, Yamamura H, Zeifman A, & Yuan JX (2011). Activity of Ca^{2+}-activated Cl^- channels contributes to regulating receptor- and store-operated Ca^{2+} entry in human pulmonary artery smooth muscle cells. Pulmonary Circulation, 1, 269–279. 10.4103/2045-8932.83447 [PubMed: 22034612]

Yamamura H, Yamamura A, Ko EA, Pohl NM, Smith KA, Zeifman A, Powell FL, Thistlethwaite PA, & Yuan JXJ (2014). Activation of Notch signaling by short-term treatment with Jagged-1 enhances store-operated Ca^{2+} entry in human pulmonary arterial smooth muscle cells. American Journal of Physiology. Cell Physiology, 306, C871–C878. 10.1152/ajpcell.00221.2013 [PubMed: 24573085]

Yoo HY, Zeifman A, Ko EA, Smith KA, Chen J, Machado RF, Zhao YY, Minshall RD, & Yuan JX (2013). Optimization of isolated perfused/ventilated mouse lung to study hypoxic pulmonary

vasoconstriction. Pulmonary Circulation, 3, 396–405. 10.4103/2045-8932.114776 [PubMed: 24015341]

Yu Y, Keller SH, Remillard CV, Safrina O, Nicholson A, Zhang SL, Jiang W, Vangala N, Landsberg JW, Wang JY, Thistlethwaite PA, Channick RN, Robbins IM, Loyd JE, Ghofrani HA, Grimminger F, Schermuly RT, Cahalan MD, Rubin LJ, & Yuan JXJ (2009). A functional single-nucleotide polymorphism in the TRPC6 gene promoter associated with idiopathic pulmonary arterial hypertension. Circulation, 119, 2313–2322. 10.1161/CIRCULATIONAHA.108.782458 [PubMed: 19380626]

Yuan JX, Aldinger AM, Juhaszova M, Wang J, Conte JV Jr., Gaine SP, Orens JB, & Rubin LJ (1998). Dysfunctional voltage-gated K^+ channels in pulmonary artery smooth muscle cells of patients with primary pulmonary hypertension. Circulation, 98, 1400–1406. 10.1161/01.CIR.98.14.1400 [PubMed: 9760294]

Yuan XJ (1995). Voltage-gated K^+ currents regulate resting membrane potential and $[Ca^{2+}]_i$ in pulmonary arterial myocytes. Circulation Research, 77, 370–378. 10.1161/01.RES.77.2.370 [PubMed: 7542182]

Yuan XJ, Goldman WF, Tod ML, Rubin LJ, & Blaustein MP (1993). Hypoxia reduces potassium currents in cultured rat pulmonary but not mesenteric arterial myocytes. The American Journal of Physiology, 264, L116–L123. 10.1152/ajplung.1993.264.2.L116 [PubMed: 8447425]

Zhang J, Dong J, Martin M, He M, Gongol B, Marin TL, Chen L, Shi X, Yin Y, Shang F, Wu Y, Huang HY, Zhang J, Zhang Y, Kang J, Moya EA, Huang HD, Powell FL, Chen Z, … Shyy JYJ (2018). AMP-activated protein kinase phosphorylation of angiotensin-converting enzyme 2 in endothelium mitigates pulmonary hypertension. American Journal of Respiratory and Critical Care Medicine, 198, 509–520. 10.1164/rccm.201712-2570OC [PubMed: 29570986]

Zhou H, Sun L, Yang XL, & Schimmel P (2013). ATP-directed capture of bioactive herbal-based medicine on human tRNA synthetase. Nature, 494, 121–124. 10.1038/nature11774 [PubMed: 23263184]

Zion O, Genin O, Kawada N, Yoshizato K, Roffe S, Nagler A, Iovanna JL, Halevy O, & Pines M (2009). Inhibition of transforming growth factor β signaling by halofuginone as a modality for pancreas fibrosis prevention. Pancreas, 38, 427–435. 10.1097/MPA.0b013e3181967670 [PubMed: 19188864]

What is already known

- Halofuginone is an analogue of febrifugine originally isolated from traditional Chinese herb Chang Shan.
- Halofuginone shows beneficial effects in treatment of malaria, cancer, fibrosis and heart failure.

What does this study add

- Halofuginone increases voltage-gated K^+ currents and decreases Ca^{2+} influx through various Ca^{2+} channels in PASMCs.
- Halofuginone attenuates hypoxic pulmonary vasoconstriction, inhibits hypoxia-induced pulmonary vascular remodelling and reverses established pulmonary hypertension.

What is the clinical significance

- Halofuginone shows promise in treatment for pulmonary hypertension by inducing vasodilation and reversing vascular remodelling.

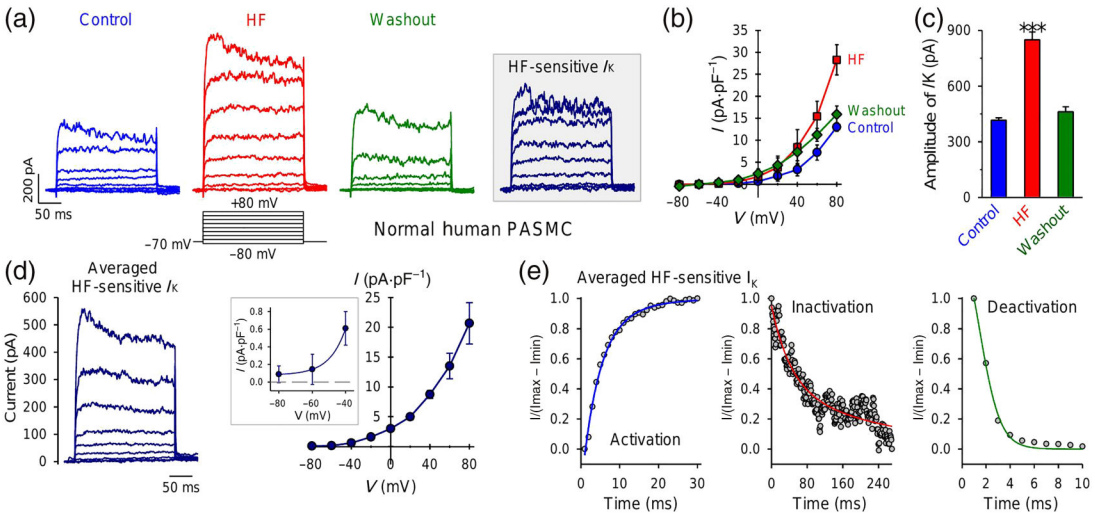

FIGURE 1.

Halofuginone (HF) reversibly increases whole-cell K^+ currents in pulmonary arterial smooth muscle cells (PASMCs). (a) Representative currents, elicited by depolarizing a cell from a holding potential of −70 mV to a series of test potentials ranging from −80 to +80 mV in increment of 20 mV, before (control), during (HF) and after (washout) extracellular application of 1-μM halofuginone. The halofuginone-sensitive K^+ currents (*IK*) shown in *inset* are obtained by subtracting the currents recorded before halofuginone application (control) from the currents recorded during halofuginone application (HF). (b) Averaged current–voltage (*I–V*) relationship curves (means ± SE, $n = 12$) for currents recorded before (control), during (HF) and after (washout) halofuginone application. The halofuginone curve is significantly different from control and washout curves. (c) Amplitude of currents at +80 mV under control, HF and washout conditions. Data shown are means ± SEM, $n = 12$. $^*P < 0.05$, significantly different from control and washout. (d) Averaged HF-sensitive I_K (left panel) and its *I–V* curve (right panel). *Inset*: enlarged portion of the *I–V* curve showing the halofuginone -sensitive I_K at negative potentials (−80 to −40 mV). (e) Activation (left panel), inactivation (middle panel) and deactivation kinetics of averaged halofuginone-sensitive I_K at +80 mV. The data were best fitted by sigmoid (four parameters) for activation, exponential decay (six parameters) for inactivation and sigmoid (three parameters) for deactivation

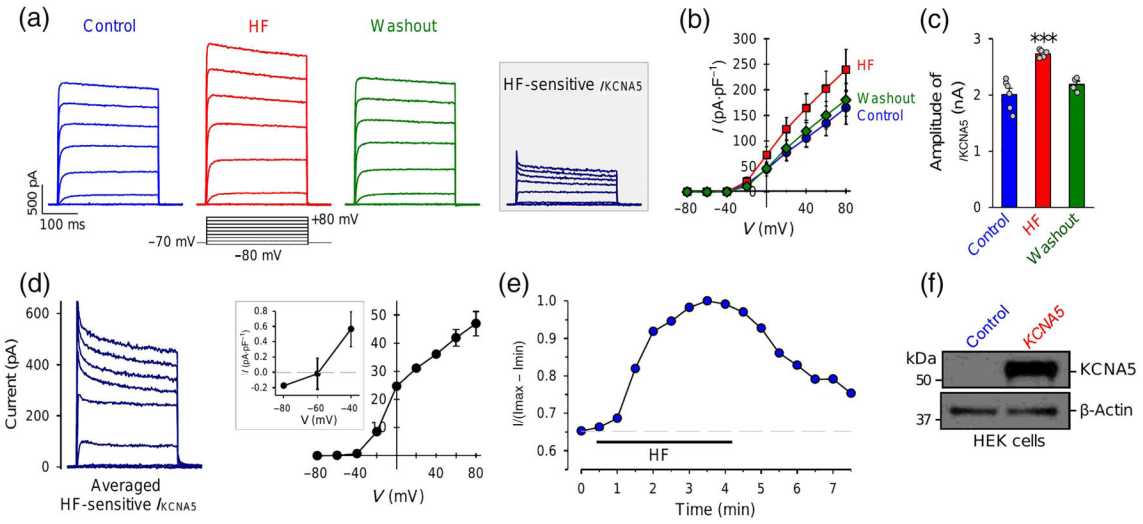

FIGURE 2.

Halofuginone (HF) reversibly increases whole-cell K^+ currents in HEK cells transiently transfected with the human *KCNA5* gene. (a) Representative outward K^+ currents, elicited by depolarizing a cell from a holding potential of −70 mV to a series of test potentials ranging from −80 to +80 mV in increment of 20 mV, before (control), during (HF) and after (washout) extracellular application of 1-μM halofuginone. The halofuginone -sensitive K^+ currents through KCNA5 channels (I_{KCNA5}) shown in *inset* are obtained by subtracting the currents recorded before halofuginone application (control) from the currents recorded during HF application (HF). (b) Averaged current–voltage (*I–V*) relationship curves (means ± SE, $n = 8$) for I_{KCNA5} recorded before (control), during (HF) and after (washout) halofuginone application. The halofuginone curve is significantly different from control and washout curves. (c) Amplitude of I_{KCNA5} at +80 mV under control, HF and washout conditions. Data shown are means ± SEM; $n = 8$ cells; for two of the 8 cells we were unable to record current after application of HF. $^*P < 0.05$, significantly different from control and washout. (d) Averaged halofuginone -sensitive I_{KCNA5} (left panel) and its *I–V* curve (right panel). *Inset*: enlarged portion of the *I–V* curve showing the halofuginone -sensitive I_{KCNA5} at negative potentials (−80 to −40 mV). (e) Time course of halofuginone -induced effect on I_{KCNA5}. Normalized I_{KCNA5} at +80 mV before, during and after extracellular application of 1-μM halofuginone. (f) Western bot analysis on KCNA5 in HEK cells transfected with an empty vector (control, $n = 6$ cells) or the human *KCNA5* gene (*KCNA5*, $n = 6$ cells)

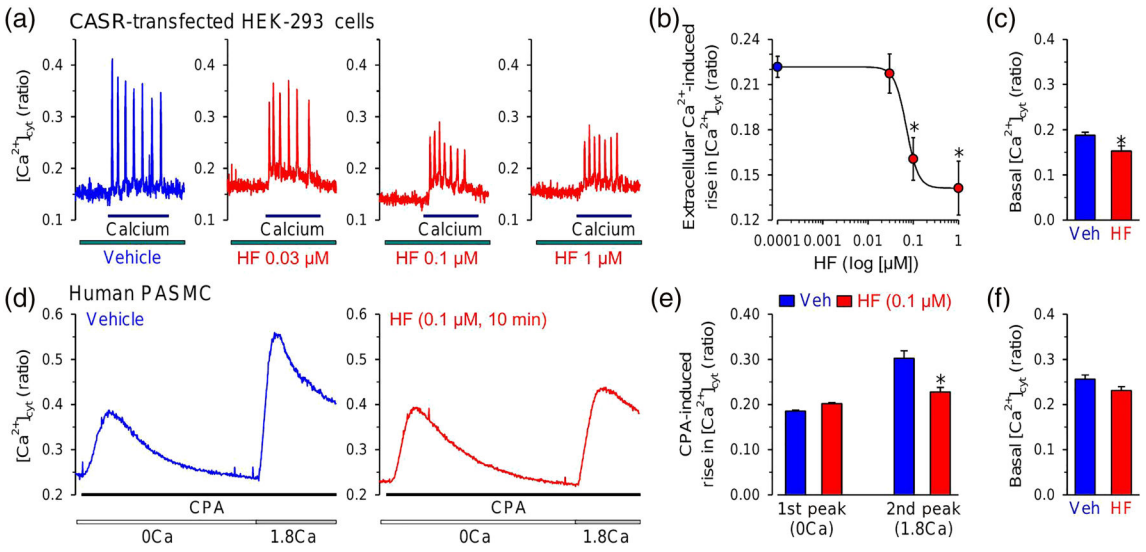

FIGURE 3.

Halofuginone (HF) inhibits receptor-operated and store-operated Ca^{2+} entry. (a) Representative traces showing changes in $[Ca^{2+}]_{cyt}$ before, during and after superfusion of extracellular application of 1.8-mM Ca^{2+} (calcium) in HEK-293 cells transfected with the calcium-sensing receptor (CaSR) gene (*CASR*) with (HF) or without (vehicle [Veh]) treatment of 0.03-, 0.1- and 1-μM halofuginone. (b) Summarized data showing the concentration–response curve of 1.8-mM Ca^{2+}-induced increases in $[Ca^{2+}]_{cyt}$ in *CASR*-transfected HEK-293 cells treated with different concentrations of halofuginone (0.0001 to 1 μM). Data shown are means ± SEM, $n = 6$ independent experiments for each data points. $^*P < 0.05$, significantly different from 0.0001-μM halofuginone. (c) Summarized data (means ± SEM) showing the basal $[Ca^{2+}]_{cyt}$ in *CASR*-transfected HEK-293 cells treated with Veh ($n = 5$) and all concentrations of halofuginone (0.03–1 μM) (HF, $n = 7$). $^*P < 0.05$, significantly different from Veh. (d) Representative traces showing changes in $[Ca^{2+}]_{cyt}$ before and during extracellular application of cyclopiazonic acid (CPA, 10 μM) in the absence (0Ca) or presence (1.8Ca) of 1.8-mM Ca^{2+} in human PASMCs shortly (10 min) treated with Veh (left panel) or 0.1-μM halofuginone (right panel). (e) Summarized data (means ± SEM, $n = 6$ independent experiments) showing the CPA-induced increases in $[Ca^{2+}]_{cyt}$ in the absence (first peak, 0Ca) and presence (second peak, 1.8Ca) of 1.8-mM extracellular Ca^{2+} in human PASMCs treated with Veh or halofuginone (0.1 μM). $^*P < 0.05$, significantly different from Veh. (f) Summarized data (means ± SEM) showing the basal $[Ca^{2+}]_{cyt}$ in human PASMCs treated with Veh ($n = 6$ independent experiments) and 0.1-μM halofuginone ($n = 6$ independent experiments)

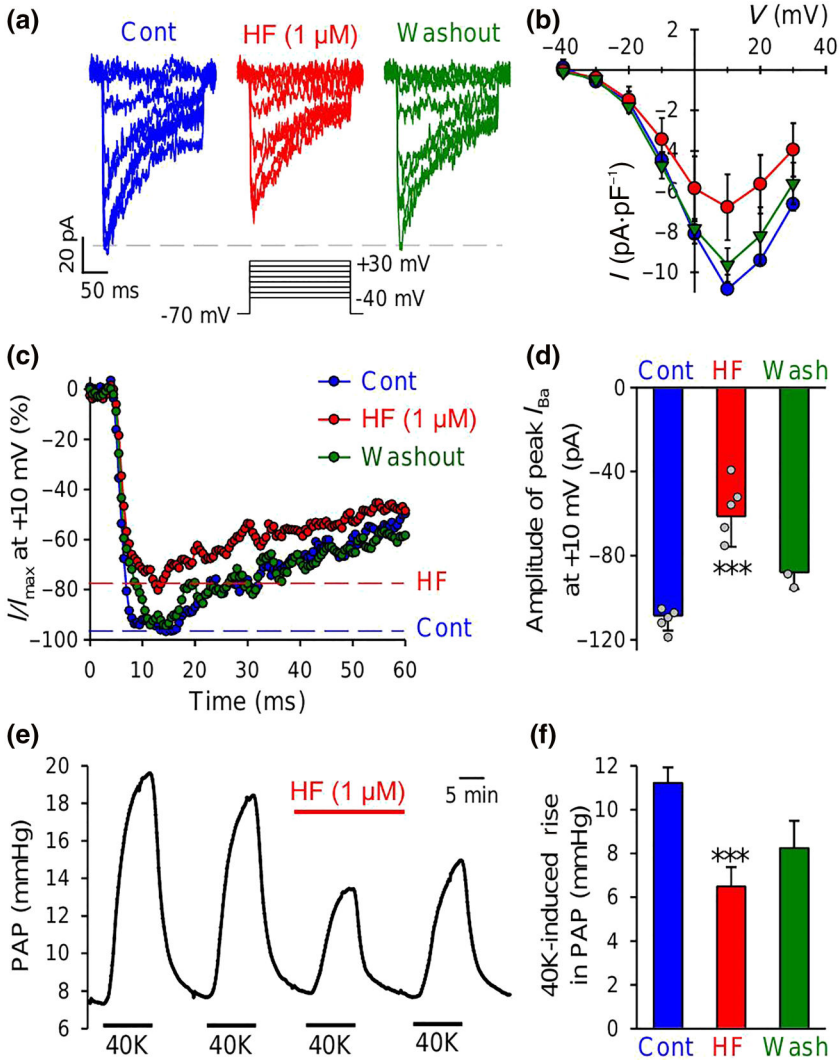

FIGURE 4.

Halofuginone (HF) reversibly decreases whole-cell voltage-gated Ca^{2+} currents (I_{Ca}) in pulmonary arterial smooth muscle cells (PASMCs). (a) Representative inward currents, elicited by depolarizing a cell from a holding potential of −70 mV to a series of test potentials ranging from −40 to +30 mV in increment of 10 mV, before (control), during (HF) and after (washout) extracellular application of 1-μM halofuginone. (b) Averaged current–voltage (*I–V*) relationship curves (means ± SEM, $n = 12$) for currents recorded before (control), during (HF) and after (washout) halofuginone application. The halofuginone curve is significantly different from control and washout curves. (c) Activation and inactivation kinetics of I_{Ca} in PASMCs before (control), during (HF) and after (washout) treatment with halofuginone. (d) Amplitude of peak inward currents at +10 mV under control, HF and wash conditions. (means ± SEM; $n = 5$ in each group. $^*P < 0.05$, significantly different from control and washout. (e) Representative records showing pulmonary arterial pressure (PAP) in isolated perfused/ventilated mouse lung before, during and after intrapulmonary superfusion of 40-mM K^+ (40K)-containing solution in the absence or presence of 1-μM halofuginone. (f) Summarized data (means ± SEM, $n = 5$ in each group) showing the 40K-

induced increase in PAP in isolated perfused/ventilated lungs before (control), during (HF) and after (wash) intrapulmonary application of 1-μM halofuginone. *$P < 0.05$, significantly different from control and washout

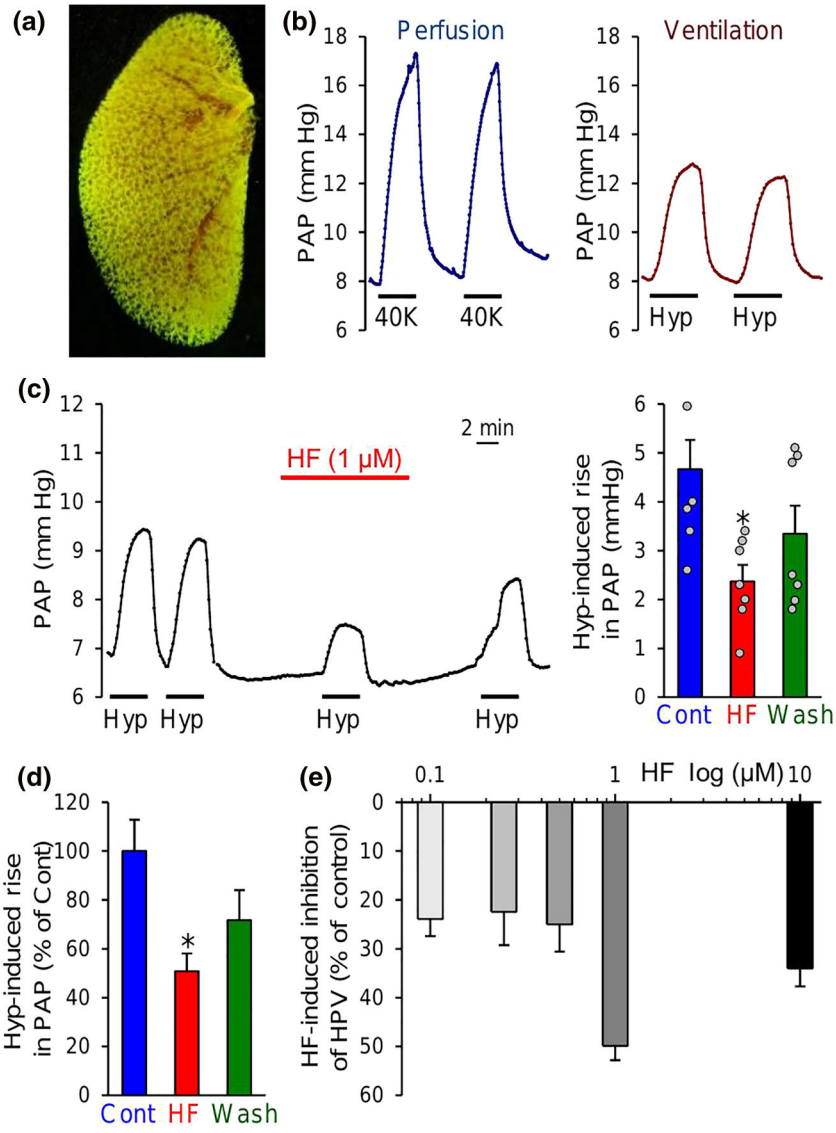

FIGURE 5.

Halofuginone (HF) inhibits acute hypoxia-induced pulmonary vasoconstriction (HPV) in isolated perfused/ventilated mouse lungs. (a) Representative lung angiogram of the left lung from a C57/BL6 mouse. (b) Representative records of pulmonary arterial pressure (PAP) in the isolated perfused/ventilated lungs before, during and after intrapulmonary perfusion with 40-mM K^+ (40K)-containing solution through a right ventricular/pulmonary arterial catheter (left panel) or ventilation with hypoxic gas (Hyp, 1% O_2 in N_2) through tracheal intubation (right panel). (c) Representative record (left panel) of PAP before, during and after ventilation with Hyp (4 min) when the lung was perfused with physiological salt solution (PSS) with (HF) or without 1-μM halofuginone. Summarized data (means ± SEM, $n = 7$ mouse lungs, right panel) showing the acute hypoxia-induced increases in PAP before (Cont), during (HF) and after (wash) before (Cont), during (HF) and after (wash) intrapulmonary application of 1 μM halofuginone. $*P < 0.05$, significantly different from Cont. (d) Normalized changes of hypoxia-induced increases in PAP before (Cont),

during (HF) and after (wash) intrapulmonary application of 1-μM halofuginone. *$P < 0.05$, significantly different from Cont (blue). (e) Concentration–response curve showing the alveolar hypoxia-induced increases in PAP in the isolated perfused/ventilated lungs with the intrapulmonary application of different concentrations of halofuginone (0.1 to 10 μM). $n = 5$ in each group

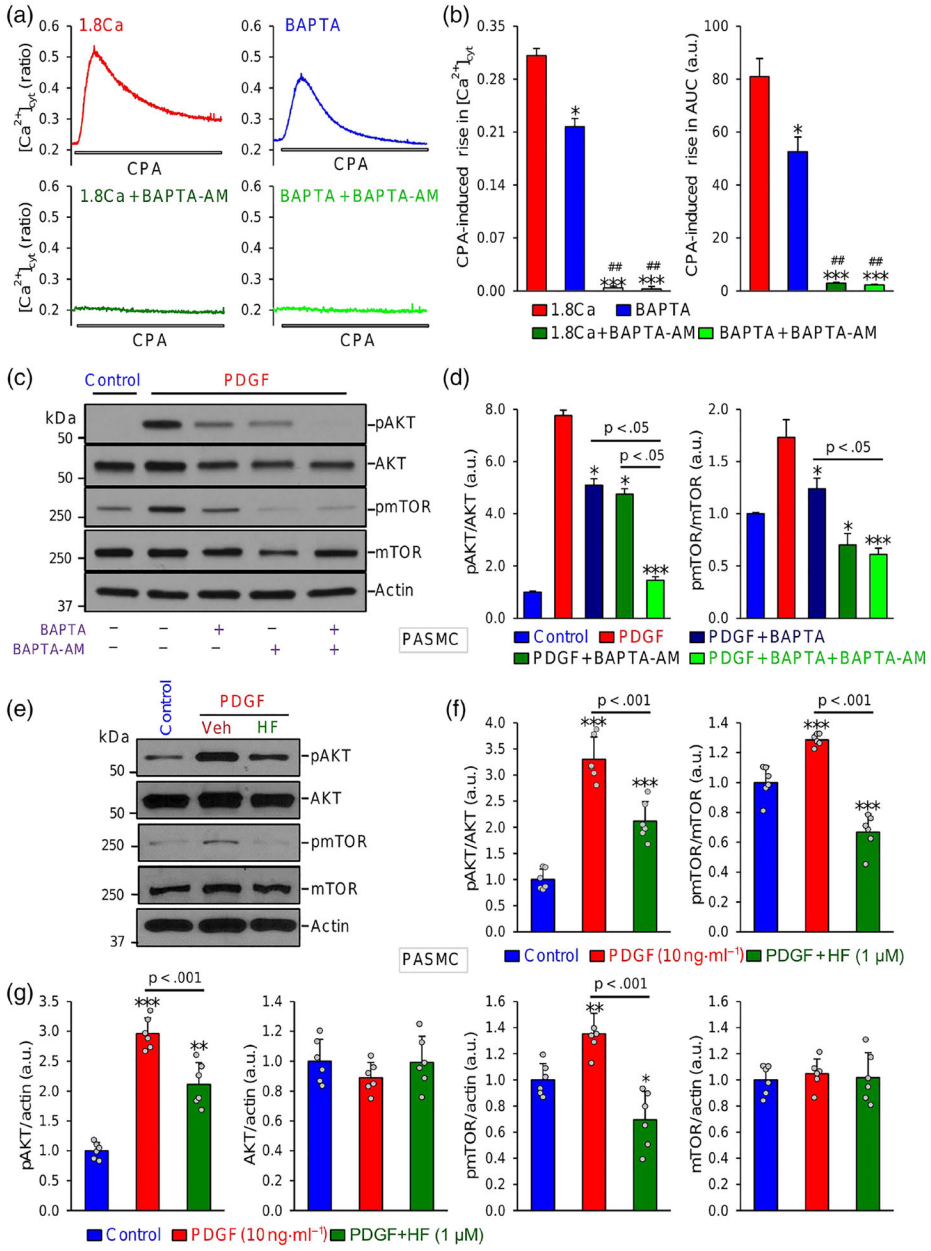

FIGURE 6.

Halofuginone (HF) inhibits Ca^{2+}-sensitive Akt/mTOR phosphorylation in human PASMCs. Representative record (a) and summarized data (b, means ± SEM, $n = 5$ independent experiments) showing cyclopiazonic acid (CPA)-induced changes in $[Ca^{2+}]_{cyt}$ in PASMCs superfused with 1.8-mM Ca^{2+} (1.8Ca)-containing solution in the absence (1.8Ca) or presence of BAPTA (BAPTA), BAPTA-AM (1.8Ca + BAPTA-AM) or BAPTA + BAPTA-AM. $^*P < 0.05$, significantly different from 1.8Ca. (c) Western blot analysis on phosphorylated Akt (pAKT), total Akt (AKT), phosphorylated mTOR (pmTOR) and total mTOR (mTOR) in control PASMCs and PASMCs treated with PDGF (PDGF-BB, 10 $ng{\cdot}ml^{-1}$) in the absence (−) and presence (+) of BAPTA or BAPTA-AM. (d) Summarized data (means ± SEM, $n = 8$ independent experiments) showing the ratio of p-Akt/Akt and p-

mTOR/mTOR in control PASMCs (control) and PDGF-treated PASMCs in the absence and presence of BAPTA or BAPTA-AM: PDGF alone, PDGF + BAPTA, PDGF + BAPTA-AM or PDGF + BAPTA + BAPTA-AM. *$P < 0.05$, significantly different from PDGF alone; #$P < 0.05$, significantly different as indicated. (e) Western blot analysis on p-Akt, Akt, p-mTOR and mTOR in control PASMCs and PASMCs treated with PDGF in the absence (vehicle control, Veh) and presence (HF) of 1-μM halofuginone (for 24 h). Summarized data (means ± SEM, $n = 5–6$ in each group) showing the ratio of p-Akt/Akt and p-mTOR/mTOR (f) as well as the relative p-Akt, Akt, p-mTOR and mTOR protein level (g, normalized to actin) in control PASMCs (control) and PDGF-treated PASMCs in the absence (PDGF) and presence (PDGF + HF) of 1-μM halofuginone. *$P < 0.05$, significantly different from control; *$P < 0.05$, significantly different from PDGF; $^{\#}P < 0.05$, significantly different as indicated.. (g) Summarized data (means ± SEM, $n = 5–6$ in each group) showing the ratio of p-Akt/Akt and p-mTOR/mTOR in control PASMCs (control) and PDGF-treated PASMCs in the absence (PDGF) and presence (PDGF + HF) of 1-μM halofuginone. *$P < 0.05$, significantly different from control; $^{\#}P < 0.05$, significantly different as indicated

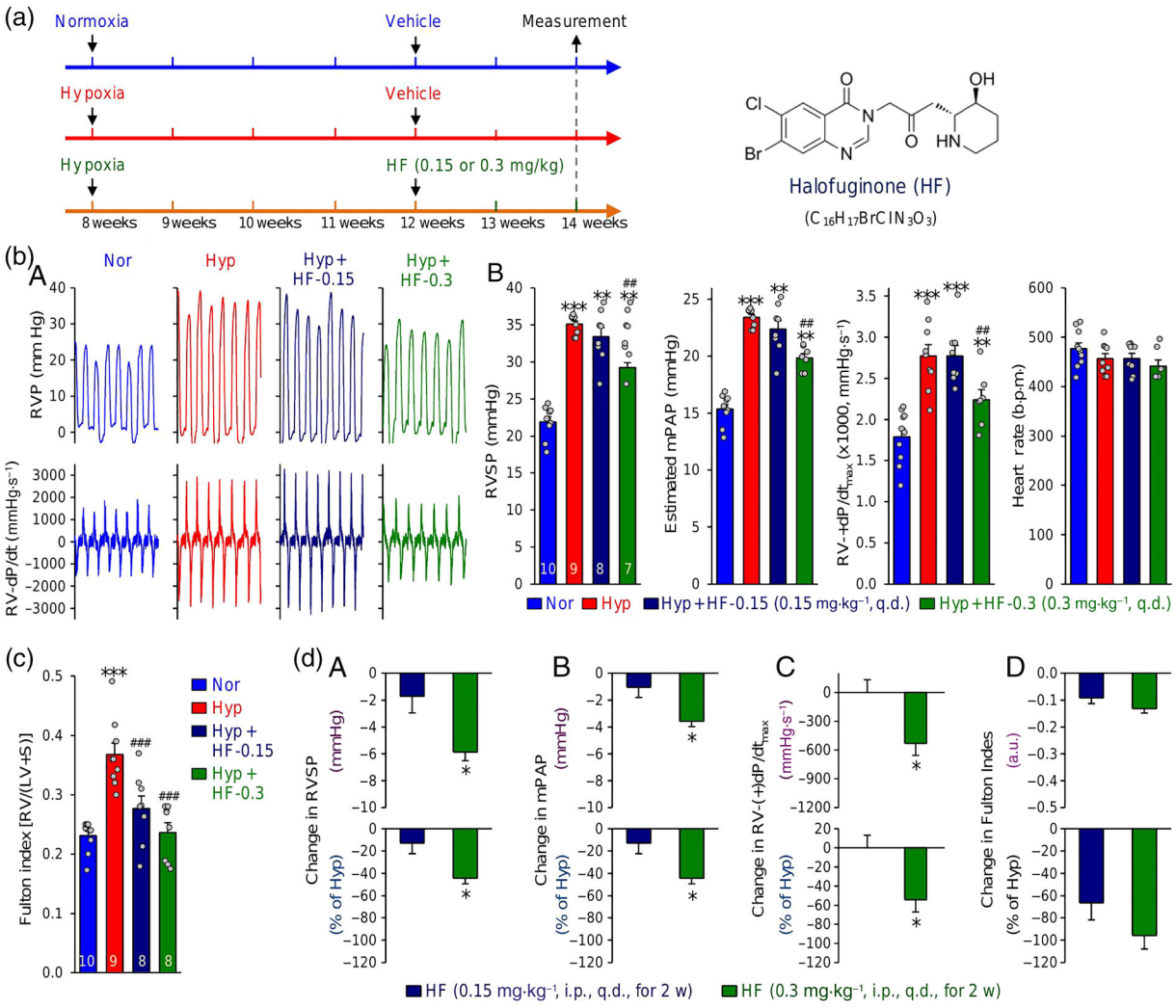

FIGURE 7.

Halofuginone (HF) partly reverses established pulmonary hypertension (PH) in mice exposed to chronic hypoxia. (a) Timeline and experimental protocol for the pharmacological experiments in mice with experimental PH or hypoxia-induced PH. Mice were divided into four groups: normoxia (Nor), hypoxia + vehicle (Hyp), hypoxia + 0.15-mg·kg^{-1} halofuginone (Hyp + HF-0.15) and hypoxia + 0.3-mg·kg^{-1} halofuginone (Hyp + HF-0.3). The Hyp and Hyp + HF mice were first exposed to hypoxia for 4 weeks and then were injected i.p. with vehicle or halofuginone at 0.15 or 0.3 mg·kg^{-1}, once a day (q.d.), for two more weeks under hypoxic conditions before haemodynamic measurements were conducted. (b) Representative records of right ventricular pressure (RVP) (A, upper panels) and right ventricular (RV) contractility (RV- ± dP/dt) (A, lower panels) in normoxic (Nor) mice, hypoxic (Hyp) mice and Hyp mice receiving i.p. administration of 0.15 mg·kg^{-1} (Hyp + HF-0.15) or 0.3 mg·kg^{-1} (Hyp + HF-0.3) of halofuginone. Summarized data (B, means ± SEM) showing right ventricular systolic pressure (RVSP), estimated mean pulmonary arterial pressure (mPAP), RV- + dP/dt$_{max}$ and heart rate in Nor, Hyp, Hyp + HF-0.15 and Hyp + HF-0.3 mice, n = 7–10 in each group. *P < 0.05, significantly different from Nor;

$^{\#}P < 0.05$, significantly different from Hyp. (c) Summarized data (means ± SEM) showing Fulton index, the ratio of the weight of RV to the weight of left ventricle (LV) and septum (S) [RV/(LV + S)] in Nor, Hyp, Hyp + HF-0.15 and Hyp + HF-0.3 mice, $n = 5$ in each group. $^{*}P < 0.05$, significantly different from Nor; $^{\#}P < 0.05$, significantly different from Hyp. (d) Summarized data (means ± SEM) showing averaged changes of RVSP (A, in mmHg and in % of Hyp), mPAP (B, in mmHg and in % of Hyp), RV- + dP/dt_{max} (C, in $mmHg \cdot s^{-1}$ and in % of Hyp) and Fulton index (D, in actual value of the ratio and in % of Hyp)

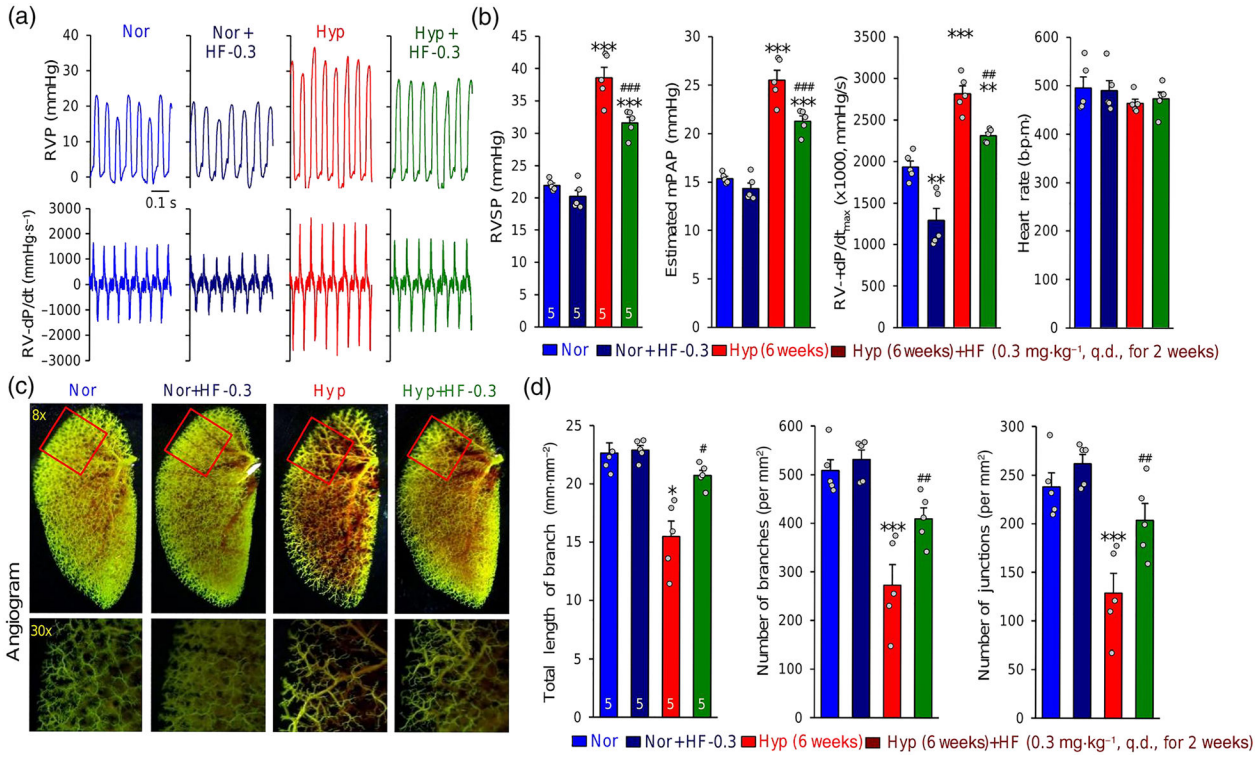

FIGURE 8.

Halofuginone (HF) partly reverses established pulmonary hypertension (PH) in mice exposed to chronic hypoxia by inhibiting pulmonary vascular remodelling. (a) Representative records of right ventricular pressure (RVP) (upper panels) and right ventricular (RV) contractility (RV- ± dP/dt) (lower panels) in normoxic (Nor) mice, Nor mice receiving intraperitoneal administration of 0.3 mg·kg^{-1} of halofuginone (Nor + HF-0.3), hypoxic (Hyp) mice and Hyp mice receiving 0.3 mg·kg^{-1} of halofuginone (i.p.) (Hyp + HF-0.3). (b) Summarized data (means ± SEM) showing right ventricular systolic pressure (RVSP), estimated mean pulmonary arterial pressure (mPAP), RV- + dP/dt$_{max}$ and heart rate in Nor, Nor + HF-0.3, Hyp and Hyp + HF-0.3 mice, $n = 5$ in each group. *$P <$ 0.05, significantly different from Nor and Nor + HF-0.3; #$P < 0.05$, significantly different from Hyp. (c) Representative lung angiograph of the left lung at 8× (upper panels) and 30× (lower panels) magnification from Nor, Nor + HF-0.3, Hyp and Hyp + HF-0.3 mice. (d) Summarized data (means ± SEM) showing the total length of lung vascular branches (left panel), the number of lung vascular branches (middle panel) and the number of vascular branch junctions (right panel) per mm^2 of area in the lungs from Nor, Nor + HF-0.3, Hyp and Hyp + HF-0.3 mice $n = 5$ in each group. *$P < 0.05$, significantly different from Nor and Nor + HF-0.3; $^{\#}p < .05$ and $^{\#}P < 0.05$, significantly different from Hyp. Eight-week-old mice were divided into four groups: normoxia (Nor), Nor + HF (0.3 mg·kg^{-1}), hypoxia (Hyp) + vehicle and hypoxia + 0.3-mg·kg^{-1} HF (Hyp + HF-0.3). The Hyp and Hyp + HF mice were first exposed to hypoxia for 4 weeks and then intraperitoneally injected with vehicle and halofuginone (0.3 mg·kg^{-1}), once a day (q.d.), for two more weeks under hypoxic conditions (total time, 6 weeks) before angiography measurements were conducted

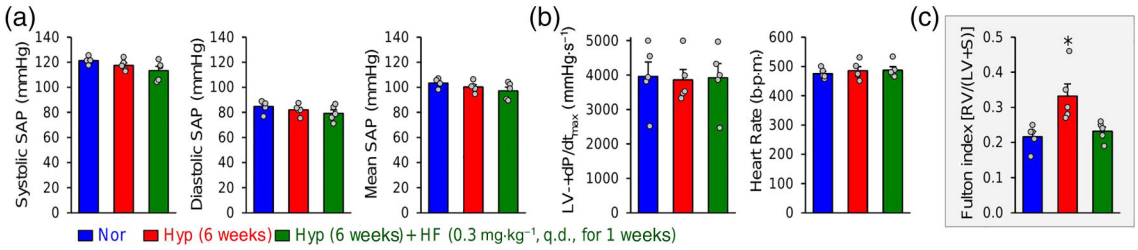

FIGURE 9.

Halofuginone (HF) did not affect systemic arterial pressure (SAP) in mice with established pulmonary hypertension (PH). Summarized data (means ± SEM) showing systolic (left), diastolic (middle) and mean (right) systemic arterial pressure (SAP, a) measured by a catheter in left carotid artery as well as left ventricle (LV)- + dP/dt_{max} (left) and heart rate (right) (b) in normoxic mice (Nor), hypoxic mice (Hyp [6 weeks]) and Hyp (6 weeks) mice receiving 0.3 mg kg^{-1} of halofuginone (i.p. and q.d. for 1 week) (Hyp [6 weeks] + HF [0.3 mg·kg^{-1}., q.d., for 1 week]). (c) Summarized data (means ± SEM) showing Fulton index, the ratio of the weight of RV to the weight of LV and septum (S) [RV/(LV + S)] in Nor, Hyp and Hyp + HF mice (n = 5 in each group). *P < 0.05, significantly different from Nor and Nor + HF mice